

Contents lists available at ScienceDirect

Journal of Controlled Release

journal homepage: www.elsevier.com/locate/jconrel





Naturally derived mucoadhesive nanosuspension for treatment of multiple staged ocular infections

Yuting Zheng ^a, Liangju Kuang ^b, Cathy Lu ^a, Steven Vo ^a, Akitomo Narimatsu ^b, Zhonghong Kong ^a, Reza Dana ^b, Nasim Annabi ^{a,c,*}

- a Department of Chemical and Biomolecular Engineering, University of California Los Angeles, Los Angeles, CA 90095, United States
- b Schepens Eye Research Institute of Massachusetts Eye and Ear, Department of Ophthalmology, Harvard Medical School, Boston, MA, USA
- ^c Department of Bioengineering, University of California Los Angeles, Los Angeles, CA 90095, United States

ARTICLE INFO

Keywords: Ocular infection Mucoadhesive nanoparticles Enhanced bioavailability Dual prophylactic and therapeutic efficacy Controlled drug release

ABSTRACT

Bacterial ocular infections pose significant risks to vision and incur substantial economic burdens worldwide. Current standards of care, such as eye drops and ointments, suffer from poor drug bioavailability (<5 %), rapid clearance, and insufficient retention, preventing dual prophylactic and therapeutic efficacy. To address these limitations, we developed naturally derived mucoadhesive gelatin methacryloyl (GelMA) nanoparticles (NPs) functionalized with phenylboronic acid (PBA), named GelMAP, for the sustained delivery of moxifloxacin (MFX), a broad-spectrum antibacterial agent. Dispersed in a custom-designed shear-thinning matrix formulated with hyaluronic acid (HA) to enhance viscosity and ocular retention, the GelMAP nanosuspension exhibited robust mucoadhesion, efficient drug loading (>70 %), and sustained in vitro drug release. Biocompatibility and bactericidal efficacy were confirmed in vitro, showing >95 % cell viability in NIH 3T3 and human corneal epithelial cells, along with notable antibacterial activity against key ocular pathogens over 7 days. In a healthy murine model, the biosafety of the nanosuspension was confirmed. The MFX-loaded nanosuspension demonstrated around 2.6-fold longer half-life in the cornea compared to commercial MFX drops (Vigamox®), indicating higher drug retention. Designed to prevent infection and treat established conditions, its efficacy was evaluated in a murine bacterial keratitis model. The MFX-loaded nanosuspension outperformed Vigamox® by reducing corneal opacity, achieving lower clinical scores (indicating better outcomes), and decreasing bacterial counts. Histological analysis showed minimal inflammation and a preserved corneal structure, validating the effectiveness of the GelMAP nanosuspension. Currently, no NP formulation has been widely demonstrated to offer dual efficacy in both early and established infections, underscoring GelMAP nanosuspension's potential for comprehensive ocular infection management by reducing treatment frequency, minimizing complications, and enhancing patient compliance.

1. Introduction

Ocular infection can cause significant damage to the eye, leading to increased morbidity and blindness worldwide [1–3]. Eye infection results in conjunctivitis, keratitis, endophthalmitis, and other complications [4]. According to the Centers for Disease Control and Prevention, one million Americans develop eye infections that require medical intervention each year, resulting in \$175 million in direct healthcare costs [5]. The most common and noninvasive methodology for treating ocular infection is topical instillation of antibiotics [6]. However, low therapeutic efficiency and patient compliance with ophthalmic

antibiotic formulations often lead to bacterial resistance and treatment failure [7]. In addition, ocular drug delivery has been challenging due to rapid tear turnover, reflex blinking, weak corneal penetration, and limited residence time, leading to low drug bioavailability (< 5 % after 15 min) [8,9]. To overcome these challenges, various methods have been developed to improve drug delivery outcomes such as adding thickening agents to the eye drops [10,11], applying drug-eluting contact lenses (CLs) [12,13], using *in situ* forming drug-loaded hydrogels [14,15], developing nanodelivery vehicles [16–18], to prolong the permanence of the medication on the eye surface.

Despite advancements in ocular drug delivery, current strategies face

E-mail address: nannabi@ucla.edu (N. Annabi).

^{*} Corresponding author.

significant limitations [19]. For example, thickening agents or ointments may increase precorneal retention time, but small drug molecules are rapidly washed away during blinking. Moreover, high viscosity can cause discomfort, irritation, and blurry vision, leading to reduced patient compliance [20]. While drug-eluting CLs can bypass issues related to high viscosity, their effectiveness heavily depends on their compositions, which dictates drug binding affinity, loading capacity, and release profile. Achieving an optimal balance remains challenging, as each drug-CL combination often necessitates a personalized design to meet specific therapeutic needs [12]. In contrast, eye drops provide more precise dosage control through simple concentration adjustments, allowing for tailored therapeutic delivery. Moreover, CLs can be complicated and uncomfortable to wear. In addition, controlling the release of drugs loaded into CLs during storage is particularly challenging, as premature drug release frequently occurs before application. Similarly, current strategies based on drug-loaded adhesive hydrogels struggle with complexity, fast drug release [21], and insufficient adhesion over time under wet conditions [22]. Our group previously developed a ciprofloxacin (CPX) eluting adhesive hydrogel based on gelatin methacryloyl (GelMA) with an in vitro CPX release profile up to 24 h [23]. While this represented an improved therapeutic efficiency compared with commercial eye drops, our strategy was impractical for frequent use by patients as it required a CL applicator and an external light device for gelation. Additionally, achieving uniform application of the liquid precursor with the medication before in situ gelation posed significant challenges. The complex handling and low tolerance for errors or readjustments of this drug-eluting bioadhesive system may also limit its usability as compared to the simplicity of eye drops. Furthermore, the use of resorbable inserts could reduce patient compliance due to the sensation of a foreign body [24]. Collectively, these technologies fail to maintain therapeutic drug concentrations over time, preventing them from simultaneously addressing infection prevention and treatment needs. This underscores their inability to deliver comprehensive ocular care.

In view of the challenges from ointment, hydrogels, or CL-based strategies, mucoadhesive nanomaterials are promising due to their superior permeability across biological membranes, increasing drug bioavailability and residence time in the eyes [7,25]. Many mucoadhesive nanoparticles (NPs)-based ophthalmic antibiotic formulations have been developed and demonstrated prolonged drug release for better therapeutic outcomes. Most of these mucoadhesive NPs developed for ocular infections are based on chitosan (Table S1) and have been widely used to load different drugs such as tedizolid phosphate [26], daptomycin [27], levofloxacin [28], and ofloxacin [29] for prolonged release. Chitosan's positive charge allows for electrostatic interactions with negatively charged mucin, promoting adhesion to the ocular surface [30]. However, these interactions are sensitive to pH fluctuations and ions in tear fluid, which can reduce NP effectiveness [31,32]. Additionally, the high surface charge of chitosan raises concerns related to cytotoxicity and immune responses [33–35], especially in sensitive ocular tissues. In general, most of the engineered mucoadhesive NPs exhibit rapid drug release, typically within 24 h, which is inadequate for sustained antibacterial treatment. Few formulations of these NPs have shown improved antibacterial effects over free drugs both in vitro and in vivo, but their biosafety remains under explored. Moreover, lack of in vivo comparisons with commercial eye drops makes it difficult to assess their clinical advantages and translation. Therefore, it is imperative to develop a biocompatible mucoadhesive nanosuspension that can effectively adhere to ocular mucosa and offer sustained antibiotic release with better therapeutic outcomes compared to commercial eye drops. In contrast to chitosan, phenylboronic acid (PBA) molecules form stable yet reversible boronate ester complexes with cisdiol groups of mucin glycoproteins at physiological pH (~7.4), supporting effective mucoadhesion under ocular conditions [36]. Due to its high affinity with glycol, PBA has found wide applications in ocular drug delivery. Numerous studies have showcased the strong

mucoadhesiveness and biocompatibility of PBA in vitro and in vivo [37-40].

In this work, we developed an ocular drug delivery system based on mucoadhesive NPs by using naturally derived biodegradable gelatin and PBA. Gelatin was first functionalized with methacrylic anhydride (MA) to form GelMA, enabling photocrosslinking for NP stabilization. GelMA was then modified with PBA to endow mucoadhesiveness to the final GelMA-PBA (GelMAP) prepolymer, which was then used to form NPs through a solvation method. The GelMAP NPs were then loaded with moxifloxacin (MFX), a broad-spectrum antibiotic, effective toward both gram-positive and gram-negative bacteria such as staphylococcus aureus and pseudomonas aeruginosa, that are mainly responsible for conjunctivitis, keratitis, and endophthalmitis. To improve ocular retention of NPs, a shear-thinning matrix with proper viscosity was developed using a combination of components, including hyaluronic acid (HA), which was included to modulate viscosity and contribute to the shear-thinning behavior, to disperse the mucoadhesive NPs and form the GelMAP nanosuspension. The synthesis of the GelMAP biopolymer was chemically verified, and NPs were characterized for size, polydispersity index (PDI), MFX encapsulation and in vitro mucoadhesion. The matrix was also assessed via rheology and wettability on mucin-coated slides. The combined NPs and matrix were tested for in vitro MFX release, antibacterial activity, ex vivo mucoadhesion, and in vitro biocompatibility. To ensure safety and drug retention, in vivo biocompatibility and pharmacokinetic studies were also conducted using a healthy murine model. The therapeutic efficacy of nanosuspension was also evaluated in a murine bacterial keratitis model, using Vigamox® eye drops as a commercial control. The engineered nanosuspension has potential for clinical translation and safe use, ensuring effective prevention and treatment of ocular infections with comprehensive and patient-centered

2. Results and discussion

2.1. Synthesis and characterization of PBA modified gelatin methacryloyl (GelMAP)

Sequential synthesis of GelMAP and the interaction between the drug-loaded GelMAP NPs and mucin layer on the eye are demonstrated in Fig. 1a. First, gelatin was functionalized with MA to form GelMA. GelMA was then subjected to chemical functionalization with PBA to yield PBA functionalized GelMA (GelMAP) prepolymer through 1-Ethyl-3-(3-dimethylaminopropyl) carbodiimide (EDC)/N-Hvdroxysuccinimide (NHS) coupling [41]. After complete purification, proton nuclear magnetic resonance (¹H NMR) was performed to confirm the chemical modification of both GelMA and GelMAP in dimethyl sulfoxide-d₆ (DMSO-d₆). As shown in Fig. 1b, a distinct PBA peak appeared at ~7.8 ppm in GelMAP but not in GelMA, while MA peaks around 5.5-6.0 ppm were observed in both samples, confirming successful functionalization. To accurately quantify the degree of PBA conjugation, we performed ¹H NMR in deuterium oxide (D₂O), as the aromatic region in DMSO-d₆ showed substantial overlap with gelatin backbone signals, limiting reliable integration [42]. In D₂O, a well-resolved aromatic peak from PBA protons at 7.5-7.8 ppm enabled accurate quantification (Fig. S1). Integration of this peak relative to the alanine methyl signal (~1.4 ppm) yielded a PBA-to-alanine ratio of 0.085. Based on the reported amino acid composition of gelatin (~9 mol% alanine) [43], along with manufacturer-reported molecular weight (50-100 kDa) and carboxyl content (78-80 mmol/100 g), the number of conjugated PBA groups per polymer chain was estimated to be approximately 3.4-6.9, corresponding to a conjugation efficiency of $\sim\!\!4.3\text{--}17.8~\%$ per GelMA backbone. This is comparable to the reported values for boronic acidmodified GelMA derivatives [44]. PBA content was not varied in this study, as prior work has demonstrated that increasing PBA density on NPs can enhance mucoadhesion through boronate-diol interactions with mucins, provided that NP colloidal stability is maintained [45].

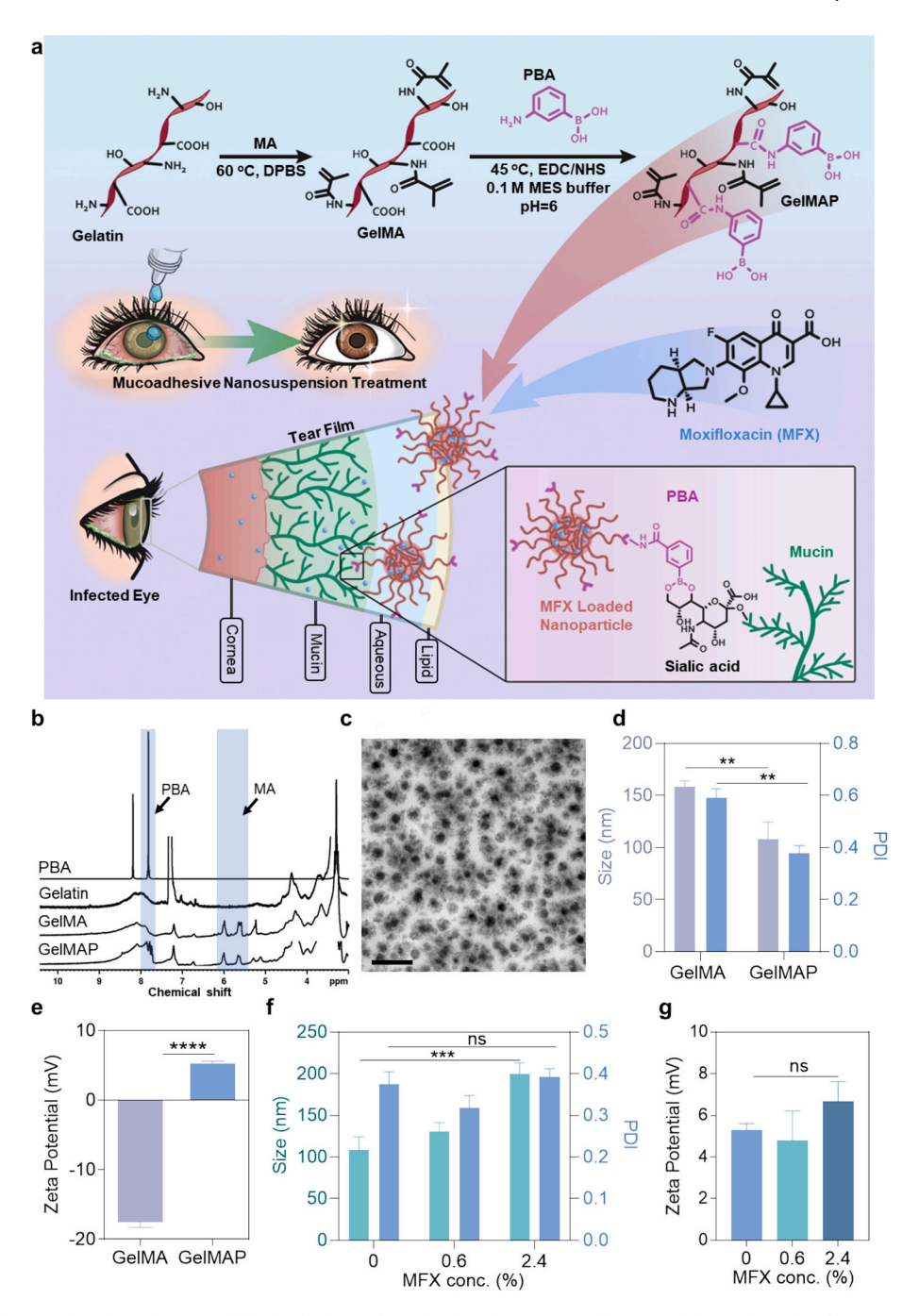


Fig. 1. Synthesis and characterization of PBA modified gelatin methacryloyl (GelMAP) prepolymer and formation of GelMAP NPs with and without MFX. (a) Schematically illustrated synthesis of GelMAP and the interaction between drug loaded GelMAP NPs and mucin of the infected eye. (b) 1 H NMR spectra of PBA, gelatin, GelMA and GelMAP in DMSO- d_{6} , demonstrating successful conjugation of MA and PBA to gelatin. (c) A representative TEM image of GelMAP NPs (scale bar = 1 µm) and their (d) hydrodynamic size, PDI, and (e) zeta potential of the GelMA and GelMAP NPs without MFX. (f) Hydrodynamic size, PDI, and (g) zeta potential of MFX-loaded GelMAP NPs at varied MFX concentrations. Error bars indicate standard deviation of the means, asterisks mark significance levels of p < 0.01(***), p < 0.001(****), p < 0.0001(****), p < 0.0001(****), p < 0.0001(*****), p < 0.0001(****)

Instead, we focused on maximizing the degree of PBA conjugation to the GelMA backbone by using an excess of EDC, NHS, and PBA during the coupling reaction to promote efficient functionalization and ensure strong mucoadhesive properties and colloidal stability.

2.2. Characterizations of GelMAP NPs with and without MFX

To study the effect of PBA functionalization on the NP characteristics, we formed both GelMA NPs (without PBA functionalization) as a control and GelMAP NPs. The morphology and size of the synthesized

GelMAP NPs were characterized using transmission electron microscopy (TEM). TEM analysis (Fig. 1c) confirmed the formation of spherical NPs with relatively uniform morphology. To further assess the size distribution, dynamic light scattering (DLS) measurements were conducted, revealing a hydrodynamic size of 108.4 ± 15.9 nm for GelMAP NPs (Fig. 1d). The higher PDI observed by DLS, compared to the relatively uniform particle size seen in TEM, is likely due to the hydrated and dynamic nature of the NPs in solution. DLS provides a population-averaged size distribution under aqueous conditions, capturing effects such as swelling and minor aggregation. In contrast, TEM offers

representative images of a small, localized, and dried subset of NPs. Additionally, to reflect the true formulation used in downstream applications, the NPs were not filtered prior to DLS measurements, which may have contributed to the broader size distribution observed [46]. It was also found that GelMAP NPs had a smaller average particle size as compared to GelMA NPs (158.57 \pm 4.38 nm) (Fig. 1d). This size reduction may be attributed to structural and behavioral changes in the GelMA biopolymer following PBA conjugation. Specifically, PBA conjugation is known to disrupt intramolecular hydrogen bonding and polymer-polymer interactions that contribute to the thermoresponsive behavior of GelMA [47]. As a result, GelMAP lost its ability to undergo thermal gelation [48]. This disruption of GelMA's native structure likely reduced polymer entanglement and aggregation during NP formation, contributing to the formation of smaller, more compact NPs. Previous studies have shown that ocular nano-delivery systems in the form of suspensions can lead to improved drug bioavailability with smaller particle sizes within the range of 10 to 150 nm [49]. Smaller particle sizes have shown enhanced diffusion through the tear film, allowing more effective penetration in the mucin layer on the eye [50]. GelMAP NPs showed a PDI of 0.38 \pm 0.03 similar to GelMA NPs with a PDI of 0.59 ± 0.03 (Fig. 1d). Surface charge density (zeta potential) of GelMAP NPs was measured using a Malvern Panalytical Zetasizer. An increase in the zeta potential of GelMAP NPs (Fig. 1e) could be attributed to the covalent conjugation of PBA to negatively charged carboxyl groups (-COO⁻) on GelMA via EDC/NHS-mediated coupling. In this reaction, PBA forms amide bonds with GelMA, consuming -COO groups without introducing new anionic functionalities at physiological pH. This change in surface chemistry results in a net decrease in negative charge and a corresponding shift toward a more positive surface potential. Consistently, GelMAP solutions exhibited a higher pH than GelMA when dissolved at the same concentration in water, indicating reduced free acidity. Additional experiments further confirmed that the isoelectric point increased from ~5.5 for GelMA to ~7.4 for GelMAP (Fig. S2), aligning with the observed zeta potential changes and supporting the conclusion that PBA conjugation reduced acidity and altered the polymer's net charge profile [44,51].

The hydrodynamic size of the GelMAP NPs after loading with MFX was characterized by DLS. As shown in Fig. 1f, the size of the NPs increased by approximately 1.8-fold when the MFX concentration increased from 0 % to 2.4 %. This increase in size could be attributed to the enhanced surface adsorption of MFX on the NPs at higher concentrations [52]. The PDI and zeta potential remained unchanged with increasing MFX concentration at a fixed pH of 7.4 across all drug-NP mixtures (Fig. 1g). To assess formulation stability, we evaluated MFX-loaded GelMAP NPs over a 28-day period at 4 °C. MFX-loaded GelMAP NPs remained physically stable, with no significant changes in particle size or PDI observed during storage (Figs. S3a–b). Furthermore, no visible aggregation or precipitation was detected (Fig. S3c), confirming colloidal stability under refrigerated conditions and supporting the formulation's suitability for future translational development.

2.3. Characterizations of eye drop matrix

For the application of engineered GelMAP NPs in treating ocular infections, designing a suitable eye drop matrix is crucial to enhance their functionality by prolonging NP contact with the ocular surface. Three criteria must be considered while developing the matrix formulation: shear thinning behavior, residence time, and pH. Shear thinning behavior can maximize the bioavailability of the medication inside the matrix. Maintaining a high viscosity at a low shear rate (open eye) increases ocular retention time while low viscosity at a high shear rate (blinking) provides comfort and prevents excessive stress to the ocular surface during blinking [53]. Additionally, viscosity and mucoadhesion of polymers in the matrix solution as well as the spreading of the drop upon instillation should be considered for optimizing the residence time and relative comfort after applying the eye drops [54,55]. The most

common eye drop solutions for dry eye have either very low viscosities (<30 cps) such as Systane Balance Lipid Layer Formula (Alcon Laboratories Inc., Geneva, Switzerland) or very high viscosities (≥300 cps) such as Refresh Optive Gel Drops (Allergan Inc.) [56,57]. Low-viscosity eye drops often have short-lived effects, and patients often use eye drops frequently to achieve relief. Alternatively, artificial tears with a higher viscosity provide a more gel-like consistency and may provide lubrication that lasts longer. However, very high viscosity may cause blurry vision and should only be applied before sleep. Therefore, eye drops with medium viscosity (60–90 cP) are preferred for dry treatments. Lastly, a proper pH in the range of 6.6 to 7.8 is necessary to avoid any discomfort after installation.

In our design, we developed matrix solutions with varying viscosity and shear thinning behavior by using different concentrations of three active ingredients: HA, abbreviated as H in Fig. 2, for providing viscosity and shear thinning behavior [58], hypromellose for providing mucoadhesion to prolong the residence time on the ocular surface [59], and glycerin, abbreviated as G in Fig. 2, as a lubricant and moisturizing agent to reduce surface tension, adjust rheology, and relieve dry irritated eyes [60]. In our formulations, 0.3 % (w/v) hypromellose was fixed in all compositions to provide mucoadhesion [61,62], while the concentrations of HA and glycerin were varied within the ranges of 0.1-0.5 % (w/v) [63] and 0.3-1 % (w/v) [64], respectively, to study their effects on viscosity, shear thinning behavior, and wettability on mucin-coated glass slides. While all the matrix compositions showed shear thinning behavior, changing the concentration of HA could tune the viscosity of the matrix (Figs. 2a, S4a-b). However, varying the concentration of glycerin had a very limited impact on viscosity compared to HA due to its small molecular weight (Figs. 2b, S4c-d). We also checked the wettability of the matrix solution on mucin coated glass slides by measuring the spreading area of the drop using a caliper. As shown in Figs. 2c-d and S5, while increasing the HA amount in matrix formulations decreased the wetting area of the matrix, enhancing glycerin had no impact. In this experiment, we observed that the viscosity of the solution played a major role in the matrix wettability. This could diminish the effect of reduced surface tension and increase spreading due to the addition of glycerin. Based on rheology and wettability experiments, we optimized the final eye drop matrix formulation using 0.5 % HA for proper viscosity (around 70-90 cps), 0.3-1 % glycerin, a clinically relevant range selected according to patients' eye condition, and 0.3 % hypromellose for mucoadhesion based on previous studies [65]. The shear-thinning behavior of our engineered nanosuspension is illustrated in Fig. 2e. Upon application to an open eye, the formulation exhibits high viscosity, enhancing precorneal retention. During blinking, the shear force reduces the viscosity, allowing the eye drops to spread evenly, thereby providing comfort and enhancing mucoadhesive interactions between the NPs and the mucin layer of the eye. Furthermore, rheological analysis showed that incorporating MFXloaded GelMAP NPs containing 0.5 % (w/v) MFX, consistent with commercial formulations, did not alter the shear-thinning behavior or viscosity of the matrix (Figs. S6a-b), confirming that NP loading at this dosage preserved the matrix's flow properties. To further evaluate the viscoelastic characteristics, oscillatory rheology was performed on both blank and NP-loaded matrices. Both formulations exhibited viscoelastic liquid behavior, with the loss modulus (G") consistently exceeding the storage modulus (G') across the tested frequency range of 1-10 rad/s at 37 °C (Fig. S7), indicating predominantly viscous behavior typical of shear-thinning polymer suspensions. G' and G" increased gradually with frequency, consistent with loosely entangled polymer networks. No significant differences in G' or G" were observed between the two groups, confirming that NP incorporation did not appreciably affect the viscoelastic properties of the matrix.

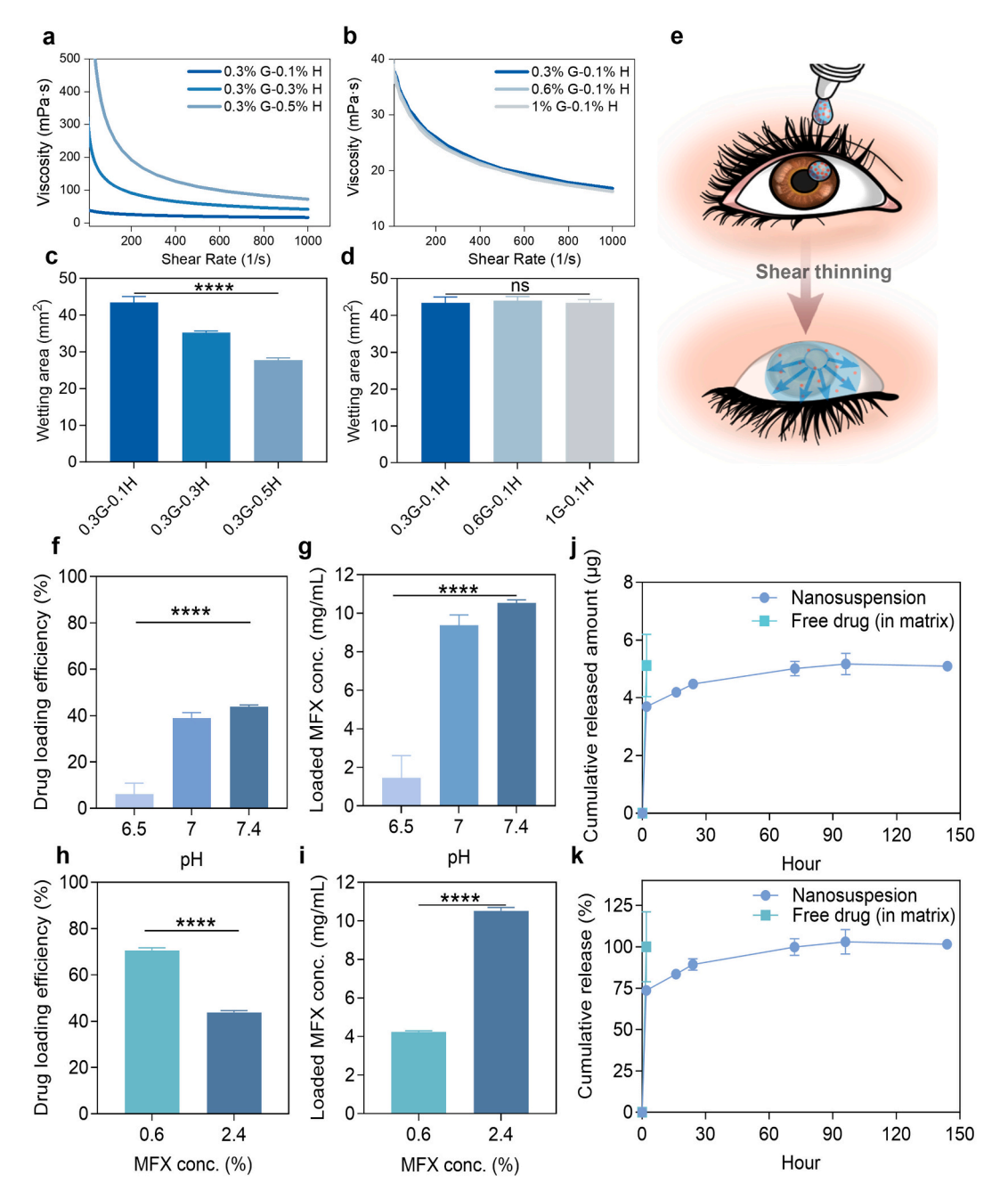


Fig. 2. Characterizations of eye drop matrix and loading efficiency, releasing profile of the MFX-loaded GelMAP NPs. Rheological studies of different matrix formulations at varied (a) HA concentrations and (b) glycerin concentrations. G stands for glycerin, H stands for HA, hypromellose was fixed at 0.3 % (w/v) for all groups. Wetting areas of different matrix formulations at varied (c) HA concentrations and (d) glycerin concentrations. (e) Schematically illustrated shear thinning behavior of the engineered nanosuspension. Upon application, it maintains high viscosity for precorneal retention. When the eye blinks, shear forces reduce viscosity, allowing even spread and enhancing mucoadhesive interactions with ocular mucin. (f) Drug loading efficiency of GelMAP NPs at different pH with a fixed MFX concentration at 2.4 % (w/v) and their corresponding (g) loaded MFX concentrations. (h) Drug loading efficiency of GelMAP NPs at different MFX concentrations at pH = 7.4 and their corresponding (i) loaded MFX concentrations. (j) Cumulative released drug amount from MFX-loaded GelMAP NPs (in matrix) and free MFX (in matrix) and their (k) cumulative release percentage over 144 h. Error bars indicate standard deviation of the means, asterisks mark significance levels of p < 0.0001 (****), ns = not significant, and $n \ge 3$.

2.4. Loading efficiency and releasing profile of the MFX-loaded GelMAP NPs

Type A gelatin has an isoionic point of 7–9 [66], and MFX has two pKas of 6.3 and 9.3 [67]. Therefore, by controlling the pH of the system, MFX could be stabilized into the GelMAP NPs through electrostatic interactions. It was found that changing the pH could influence the MFX loading efficiency. As shown in Fig. 2f, increasing pH from 6.5 to 7 increased the loading efficiency of MFX from 6.08 \pm 4.81 % to 39.08 \pm

2.24 %. Further improvement (43.86 \pm 0.71 %) was observed when increasing the pH to 7.4. This trend suggests that higher pH enhances charge complementarity between MFX and the NPs, thereby strengthening electrostatic interactions and promoting drug loading [68], as the overall repulsion between the like-charged partners of MFX and NPs would be minimal at this pH [69]. To further investigate this behavior, we measured the zeta potential of both MFX and GelMAP prepolymers at pH 5.0, 6.5, and 7.4. MFX exhibited a shift from a net positive charge at low pH to a slightly negative charge near physiological pH, consistent

with its zwitterionic nature and the pH-dependent ionization of both its acidic and basic functional groups (Fig. S2). Although MFX is typically described as zwitterionic or slightly cationic at Dulbecco's phosphate buffered saline (DPBS) buffer, our measurements in Milli-Q water showed a slightly negative surface potential under these conditions. Since the NPs were formulated in Milli-Q water, zeta potential measurements were also conducted in the same medium to maintain consistency with the formulation conditions. The use of Milli-Q water, as a low ionic strength, unbuffered medium, can increase the sensitivity of zeta potential measurements to subtle variations in surface chemistry and solution conditions, which may contribute to the observed values alongside the presence of surface-exposed carboxylate groups. GelMAP also exhibited a modest decrease in zeta potential from pH 6.5 to 7.4 but retained a slightly positive surface charge at physiological pH. The resulting charge difference between GelMAP and MFX at pH 7.4 may promote electrostatic interactions, contributing to the observed increase in drug loading efficiency (Fig. S2). Additionally, the pH of GelMAP solution (6.5) in water was notably higher than that of GelMA (5.05), reflecting reduced free carboxyl content due to PBA conjugation. This less acidic environment may further facilitate favorable electrostatic interactions with deprotonated MFX, enhancing encapsulation efficiency. Accordingly, a higher concentration of MFX (10.53 \pm 0.17 mg/ mL) could be loaded into the GelMAP NPs by increasing the pH of the mixture to 7.4 (Fig. 2g). Additionally, changing the MFX concentration could also vary loading efficiency. Increasing the MFX concentration from 0.6 % to 2.4 % reduced the loading efficiency from 70.58 \pm 1.14% % to 43.86 \pm 0.71 % but increased the final loading concentration from 4.23 ± 0.07 to 10.53 ± 0.17 mg/mL (Figs. 2h and i). This demonstrated the adjustability of the dosage in our engineered NP platform. In addition to electrostatic attraction, other non-covalent interactions may contribute to MFX loading into GelMAP NPs. MFX contains hydroxyl, ketone, and amine groups capable of forming hydrogen bonds with functional groups on the gelatin-based matrix. Hydrophobic and π - π interactions between the aromatic rings of MFX and PBA moieties on GelMAP may also facilitate drug association. Together, these interactions likely enhance the overall drug loading efficiency.

The releasing profile of the MFX-loaded GelMAP NPs was obtained using a dialysis method [70] under sink conditions. Specifically, the MFX-loaded NPs and free MFX were separately dispersed in the matrix solution at a 1:1 ratio and placed in a dialysis bag (10 k \sim 12 k MW). The releasing condition was set to 37 °C and 70 rpm shaking speed. As shown in Figs. 2j and k, all the free MFX released 100 % of the total MFX within 2 h, whereas the MFX-loaded GelMAP nanosuspension showed the initial burst phase, followed by a sustained release phase for up to 96 h. The initial burst release observed from the MFX-loaded GelMAP nanosuspension is likely due to ionic dissociation of loosely bound drug from the NP surface upon exposure to DPBS release media under sink conditions. This phenomenon is frequently observed in NP systems with surface-associated drugs and may offer therapeutic benefit in the context of ocular infections. A rapid rise in local drug concentration is critical for promptly suppressing bacterial growth and preventing colonization during the early phase of infection [71]. Following this initial burst (~75 % cumulative release within 2 h), a slower, sustained release phase was observed, extending up to 144 h. To gain insight into the mechanism governing this prolonged release, we fitted the post-burst data (2-144 h), corresponding to the encapsulated drug fraction, to the Korsmeyer–Peppas model described by the equation $\frac{M_t}{M_{\infty}} = Kt^n$, where $\frac{M_t}{M_{\infty}}$ is the fraction of drug released at time t, K is the release rate constant incorporating structural and geometric characteristics of the system, and n is the release exponent. Although we acknowledge that the model is traditionally applied to the initial 60–70 % of release, we used it here to approximate the mechanism governing the sustained release phase and to provide qualitative insight into the release behavior of the encapsulated drug. The model showed a strong fit $(R^2 = 0.98)$ with a release exponent n = 0.078, indicating a Fickian diffusion mechanism [72]. This

analysis suggests that the sustained release of MFX is primarily governed by passive diffusion from the NP matrix. Together, this biphasic profile enabled both immediate and prolonged drug exposure, which are desirable for maximizing therapeutic efficacy while minimizing dosing frequency.

2.5. Mucoadhesive characterizations of the synthesized GelMAP NPs

Mucoadhesion is crucial for ocular drug delivery as it enhances NP retention on the eye's surface, prolonging ocular drug retention time, improving absorption, and reducing clearance by tears and blinking [73,74]. This leads to increased drug bioavailability, targeted delivery, minimized dosing frequency, and better therapeutic outcomes for effective treatment of ocular diseases [75,76]. The mucoadhesive properties of GelMAP NPs were evaluated *in vitro* by using five different standard methods including DLS/zeta potential, atomic force microscopy (AFM), fluorescence-based measurement, turbidity assay, and Periodic acid/Schiff (PAS) assay.

One of the most common in vitro techniques for assessing the mucoadhesion of charged nanocarriers is zeta potential measurement, which is used to approximate the surface charge of NPs. Corneal mucins hold a relatively high negative charge based on the high prevalence of anionic sialic acid groups in mucin; as such, by monitoring the change in the zeta potential upon adhesion of anionic mucin proteins to the surface of nanocarriers, the presence of mucoadhesive interactions can be measured [76]. Such measurements are particularly beneficial to assess mucin-cationic NP interactions and have been used to assess mucoadhesive interactions between a range of cationic NPs and corneal mucins based on the reduction or reversal of the native cationic NP charge upon mucin binding [31,77]. To measure these interactions, we mixed commercially available porcine gastric mucin solution (1 mg/mL) with varying concentrations of GelMAP NPs and incubated the mixtures at $37\,^{\circ}\text{C}$ with shaking for 1 h. We also used GelMA NPs as a control. Porcine gastric mucin was used in this study as it is commonly employed as a model for preliminary mucoadhesion evaluations [78–80], owing to its availability and glycosylation features resembling those of native mucosal surfaces. The zeta potential of mucin in the incubation system was then employed to predict the mucin binding capacity of the formulations, thereby assessing the mucoadhesive performance. As shown in Figs. 3a-b, the zeta potential of GelMAP NPs increased with increasing NP concentrations, demonstrating a strong interaction with mucin due to the presence of PBA groups on NPs. In addition, electrostatic interactions between GelMAP NPs and mucins also played a role. At a higher concentration, more NPs adhered onto the mucin molecules and therefore neutralized the negative charge of the mucin to a greater extent [31]. However, the zeta potential of GelMA NPs did not show any trend with increasing NP concentrations, which could be due to the absence of PBA on the NPs. Moreover, an increase in the average size of GelMAP NPs in mucin (0.5 % GelMAP was mixed with 0.05 % (w/v) mucin) demonstrated that a strong aggregation of particles occurred upon mixing due to strong interactions between mucin and GelMAP with increased PDI (Figs. 3c-d). Compared to GelMAP NPs, GelMA NPs did not form significantly larger aggregates, confirming a lack of interactions with mucin (Fig. 3e).

Another common method to characterize mucoadhesiveness is using AFM [81]. AFM can image surfaces using a cantilever-mounted tip to scan the topography of a specimen. In our experiments, mucin was first spin-coated to mica substrate, followed by incubating with NPs for 1 h. Afterward, the mica substrate was washed three times followed by overnight drying in a desiccator before performing AFM. A stronger NP-mucosal layer interaction resulted in a higher and rougher surface after washing [82] (*i.e.*, more NPs adhered to the surface (Figs. 3f-g)). The quantitative image analysis showed that the average roughness (Ra) was significantly greater in GelMAP NPs/mucin (12.53 \pm 3.27 nm) as compared to GelMA NPs/mucin (2.41 \pm 0.22 nm). In addition, the height of the GelMAP NPs/mucin (Fig. 3giii) was more than 10 times

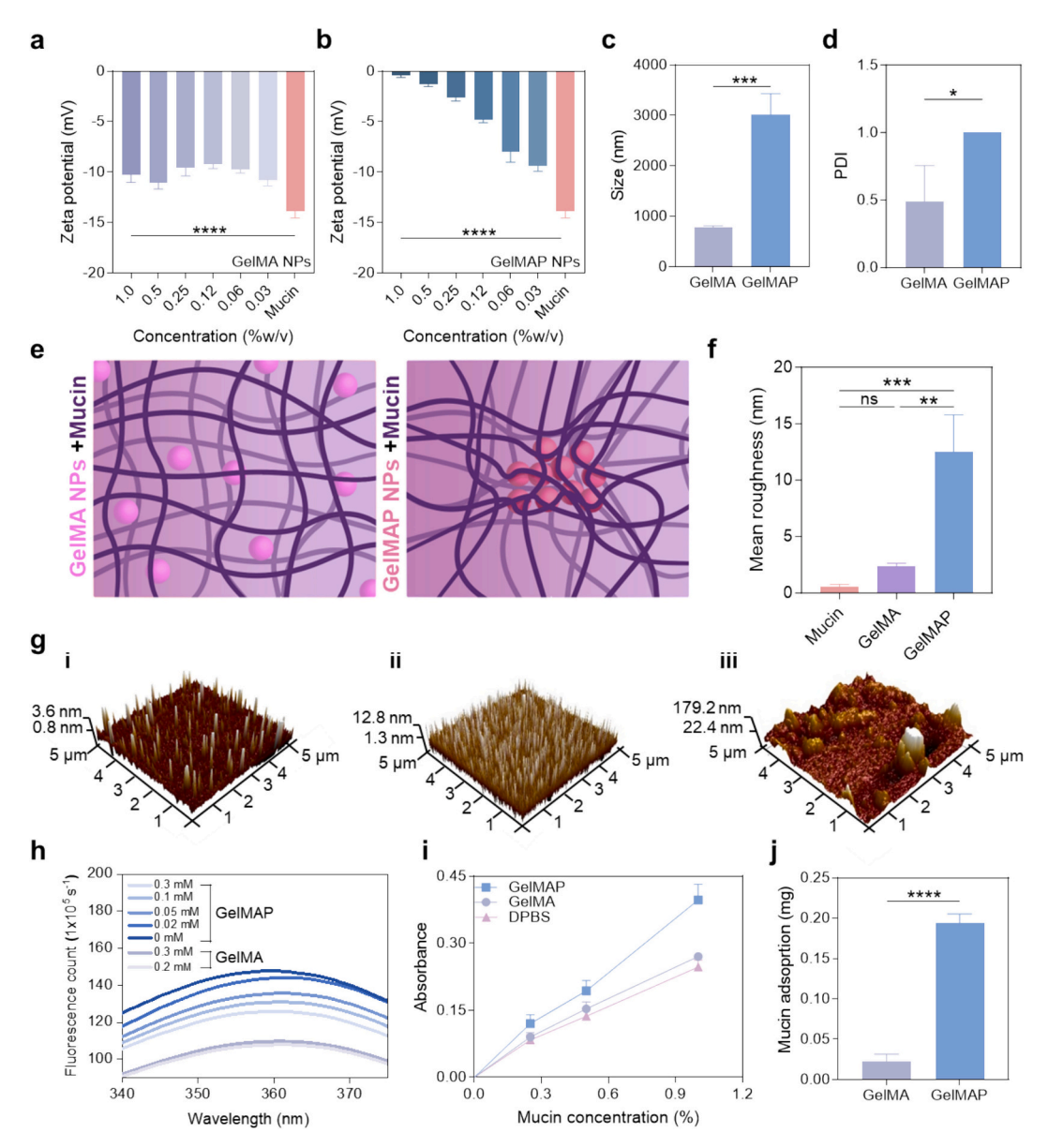


Fig. 3. *In vitro* mucoadhesion characterizations of GelMAP NPs. Zeta potential measurements of (a) GelMA and (b) GelMAP NPs on mucin solution. (c) Hydrodynamic size and (d) PDI of GelMA and GelMAP NPs mixed with mucin. (e) Schematically illustrated interactions of GelMA or GelMAP NPs with mucin. (f) Mean roughness of NP-mucin coated mica substrate after washing. (g) Representative AFM images of (i) mucin, (ii) GelMA NPs + mucin and (iii) GelMAP NPs + mucin. (h) Fluorescence spectrometer measurement of GelMAP and GelMA NPs mixed with different concentrations of sialic acid solutions. (i) Turbidity of mucin solutions at different concentrations (0.25 %, 0.5 %, 1 %) treated with GelMA NPs, GelMAP NPs and DPBS. (j) Mucin adsorption to GelMAP or GelMA NPs as determined through PAS staining. Error bars indicate standard deviation of the means, asterisks mark significance levels of p < 0.05 (*), p < 0.01(***), p < 0.001(***), p < 0.001(***)

higher than the GelMA NPs/mucin (**Fig. 3gii**) and mucin only (**Fig. 3gi**). These data together confirm stronger mucoadhesion properties of GelMAP NPs.

A high proportion of human ocular mucin sugar chains terminate in negatively charged sialic acid which can form strong cis-diol interactions with PBA [83]. Therefore, we determined the mucoadhesiveness of the GelMAP NPs with sialic acid by a fluorescent spectrometer. PBA exhibits an intrinsic fluorescence property which can be quenched when PBA forms covalent bonds with diol groups. These interactions can be investigated via a fluorescent spectrometer to assess the binding of PBA and other diol species such as sialic acid. The emission of GelMAP NPs (1 % (w/v)) before and after mixing with various sialic acid solutions at physiologically relevant concentrations (0, 0.01, 0.02, 0.03, 0.05, 0.1, 0.2, 0.3 mM) [84] was measured by a fluorescent plate reader. It was found that when GelMAP NPs were

mixed with an increased number of sialic acids, the fluorescence of the solution was gradually quenched (Figs. 3h and S8), such a trend was not observed in GelMA NPs. This result showed that the synthesized GelMAP NPs could bind efficiently to sialic acid in the mucin.

Turbidity measurement can be used to assess mucoadhesion when microaggregates form due to the interaction between NPs and mucin [76,85]. In our study, we measured absorbance values or turbidity using UV–vis spectrophotometry to qualitatively assess mucin-NP interactions. As shown in Fig. 3i, GelMAP NPs showed the highest absorbance compared with GelMA NPs and DPBS at all mucin concentrations (0.25, 0.5, and 1 %), confirming their strong mucoadhesiveness.

Finally, a PAS assay was adopted to further characterize the mucoadhesive properties of the engineered GelMAP NPs. The degree of complexation between NPs and mucin can be quantified through a color change which is detectable using a UV–vis spectrophotometer. After

mixing NPs with mucin, the free residual mucin can interact with the PAS staining kit to create a purple-magenta color, thereby showing how much mucin bonds with the NPs [38,76]. As shown in Fig. 3j, GelMAP NPs demonstrated a significantly higher mucin absorption as compared to GelMA NPs, confirming their excellent mucoadhesiveness endowed by the presence of PBA.

Mucoadhesion enhances ocular drug delivery by prolonging NP

retention, improving absorption, reducing tear clearance, and increasing bioavailability for sustained treatment. However, a comprehensive analysis of existing mucoadhesive NPs (summarized in **Table S1**) is lacking. To address this, we extensively characterized our platform, confirming its strong mucoadhesive properties and potential for improved ocular drug delivery and therapeutic outcomes.

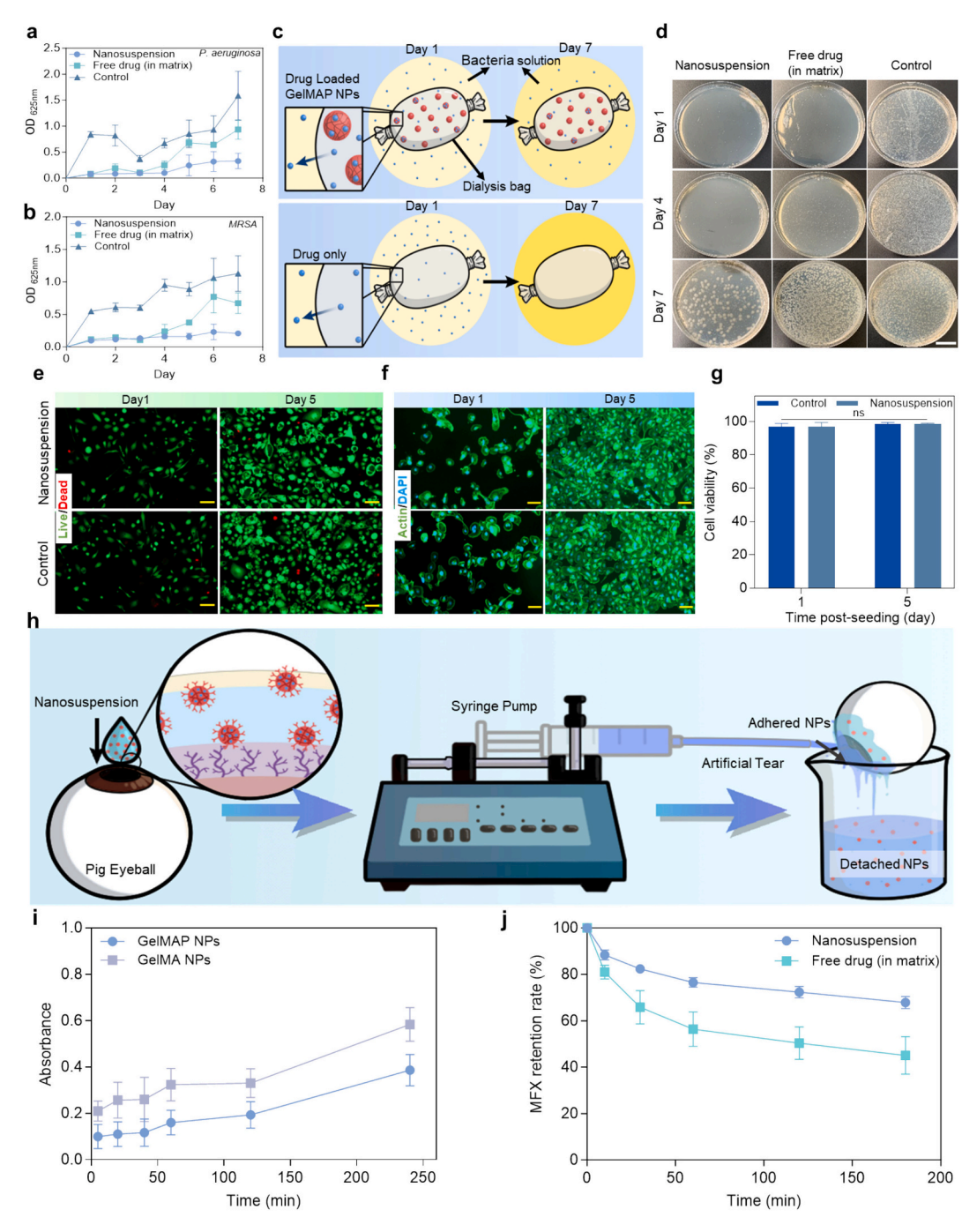


Fig. 4. *In vitro* antibacterial efficacy, biocompatibility, and *ex vivo* retention of GelMAP nanosuspension with or without MFX. Optical density (625 nm) of (a) *pseudomonas aeruginosa* and (b) *MRSA* treated with MFX-loaded GelMAP NPs (in matrix) and free MFX (in matrix) as compared with the control. (c) Schematically illustrated prolonged bactericidal effects of MFX-loaded GelMAP nanosuspension as compared to MFX (in matrix) only at the same MFX concentration (1.2 % (w/v)). (d) Digital images of *pseudomonas aeruginosa* solution with different treatments after spreading to agar plates for visualizing colonies after 3-log dilution (scale bar = 20 mm). Representative (e) Live/Dead images and (f) F-actin/DAPI stained images of HCE cells seeded on the underside of 48 well plates incubated with GelMAP NPs dispersed in matrix 1- and 5-days post-seeding (scale bars = 100 μ m). (g) Quantification of HCE cells viability over 5 days of culture. (h) Schematically illustrated *ex vivo* drug retention experiment. (i) The absorbance-time curve of GelMAP and GelMA NPs loaded with Rhodamine B in the release media and (j) the drug retention rate-time curve of MFX-loaded GelMAP nanosuspension as compared with free MFX (in matrix) in isolated pig eyeballs. Error bars indicate standard deviation of the means, ns = not significant, and $n \ge 4$.

2.6. In vitro antibacterial characterizations of the MFX-loaded GelMAP nanosuspension

Given the prolonged release profile of the mucoadhesive MFX-loaded GelMAP nanosuspension, we hypothesize that the designed NPs can kill bacteria over longer time spans compared to free MFX. To evaluate this, we performed an in vitro antibacterial test using matrix solutions containing either MFX-loaded GelMAP NPs or free MFX at the same concentration (4.8 mg in 0.4 mL) as a positive control. The samples were placed in dialysis bags (10 k \sim 12 k MW) and submerged into the bacterial solution with an optical density (OD) of 0.07-0.09 for both grampositive bacteria (methicillin-resistant staphylococcus aureus (MRSA)) and gram-negative bacteria (pseudomonas aeruginosa), responsible for the most ocular infections [86]. After incubation at 37 °C for 24 h, bactericidal effects were assessed using a plate reader and afterwards, the dialysis bags were immediately transferred to fresh bacteria solution (OD: 0.07-0.09) to further assess their ability to kill bacteria. The antibacterial effects of the MFX-loaded GelMAP nanosuspension and free MFX were assessed for up to 7 days, and the bacteria solution with no treatment was used as a control. As shown in Figs. 4a-b, S9a and S10, both free MFX and MFX-loaded GelMAP nanosuspension showed antibacterial effects against bacteria up to day 3. The free MFX could not effectively kill bacteria past day 4 whereas MFX-loaded GelMAP nanosuspension inhibited bacteria growth throughout the experiment (7 days). The experiment was stopped on day 7 due to degradation or damage of cellulose-based dialysis bags in bacteria solution over time. The extended antibacterial efficacy observed with our engineered MFXloaded GelMAP nanosuspension could be primarily due to the sustained release of MFX over a 7-day period, which contrasted with the rapid release and subsequent decline in activity observed with free MFX (Fig. 4c). The images of bacteria solution with different treatments, after being spread onto agar plates further confirmed the prolonged antibacterial efficiency of MFX-loaded GelMAP nanosuspension for both gram-positive and gram-negative bacteria. In accordance with the OD value, MFX-loaded GelMAP nanosuspension showed a more effective antibacterial effect compared with free drugs at day 4 and continued to inhibit bacterial growth up to day 7 (Figs. 4d and S9b).

Sustained antibacterial activity is crucial for treating ocular infections. Due to the prolonged release of our GelMAP NPs, we observed antibacterial effects lasting over 7 days. While other mucoadhesive NPs (summarized in **Table S1**) demonstrate short-term antibacterial activity (\leq 24 h), their long-term efficacy remains largely uncharacterized. These findings highlight the potential of our nanosuspension for sustained antibacterial treatment, addressing a critical gap in long-term ocular infection management. MFX acts by inhibiting bacterial DNA gyrase and topoisomerase IV—enzymes vital for DNA replication and transcription [87]. While this mechanism is well established, future studies will investigate how NP–bacteria interactions, mucoadhesion, and site-specific drug release contribute to the enhanced and sustained therapeutic performance of the MFX-loaded GelMAP nanosuspension.

2.7. In vitro biocompatibility of the GelMAP NPs and matrix

In vitro biocompatibility of the GelMAP nanosuspension was evaluated using NIH 3T3 cells as this cell line is most commonly used for assessing biomaterial cytotoxicity according to the International Organization for Standardization (ISO) 10993–5 [41]. Before evaluating the biocompatibility of nanosuspension, we assessed the biocompatibility of both the GelMAP NPs and the engineered matrix independently. Each component was added separately to the culture media in a well plate seeded with 3T3 cells. Cells without any treatment served as control. A Live/Dead assay demonstrated excellent cellular viability (>95 %) for both the GelMAP NP and control group up to 5 days post-seeding (Figs. S11a-b). Fluorescent F-actin and cell nuclei staining confirmed spreading and proliferation of the cells exposed to NPs up to 5 days post-seeding. As shown in Fig. S11c, GelMAP NPs supported cytoskeletal

filament spreading comparable to the no-treatment group. Cell metabolic activity was further investigated using a PrestoBlue assay. When added to cells, the PrestoBlue reagent is modified by the reducing environment of healthy cells and turns red [88], which can then be quantified using a fluorescence plate reader. As shown in Fig. S11d, the 3T3 cells exposed to NPs showed proliferation over 7 days and demonstrated no difference compared with the control group, confirming the biocompatibility of the GelMAP NPs. We also evaluated the biocompatibility of the matrix solution separately by adding it to 3T3 cells cultured in a well-plate. As shown in Figs. S12a-d, the matrix solution did not pose any cytotoxicity effects on 3T3 cells as confirmed by Live/Dead, F-actin/cell nuclei staining, and Prestoblue assay.

We next evaluated the *in vitro* biocompatibility of the nanosuspension (NPs + matrix solution). Since the nanosuspension was designed for treating ocular infections, human corneal epithelial (HCE) cells were used to further evaluate biocompatibility. The HCE cells were seeded in well plates, and GelMAP nanosuspension was added to the cell culture media. Live/Dead and Actin/DAPI assays were then performed to examine the cellular activities. As shown in Figs. 4e-g, GelMAP nanosuspension did not exhibit cytotoxic effects on HCE cells. Compared to the control group, cell viability and proliferation remained unaffected, indicating that GelMAP nanosuspension was safe and supported HCE cell growth.

2.8. Ex vivo mucoadhesive characterizations of the GelMAP nanosuspension

To further evaluate the mucoadhesive properties of the GelMAP NPs on ocular surfaces, an *ex vivo* experiment was carried out using freshly isolated pig eyeballs (Figs. 4h-j). To better visualize the prolonged retention effects due to the presence of PBA, GelMAP NPs were first loaded with a hydrophilic red dye, Rhodamine B, and then applied to the eyeballs. GelMA NPs loaded with Rhodamine B served as a control. After incubation for 30 min, eyeballs were immersed in artificial tear fluid to let the NPs detach from the ocular surface. At each predetermined time point, the absorbance at 550 nm, a wavelength corresponding to Rhodamine B, was recorded for the artificial tear fluid to evaluate the retention effects of the GelMAP NPs. As shown in Fig. 4i, mucoadhesive GelMAP NPs demonstrated a lower absorbance over 240 min compared with GelMA NPs, showing that more NPs presented on the ocular surface over time instead of the surrounding tear fluid.

To further assess the ex~vivo mucoadhesion of the engineered nanosuspension, we evaluated the drug retention curve of MFX-loaded Gel-MAP nanosuspension and compared it to that of free MFX (in matrix). In this experiment, fresh pig eyeballs were treated with 200 μL of the matrix solution containing MFX-loaded GelMAP NPs or free MFX. After 15 min, the eyeballs were washed vertically with artificial tear fluid at a rate of 0.5 mL/min by using a syringe pump (Fig. 4h). The washing solution was collected at different time points. The content of MFX in the washing solution was quantified using a UV–vis spectrophotometer. As shown in Fig. 4j, MFX-loaded GelMAP NPs showed a significantly higher drug retention rate (67.91 \pm 2.61 %) as compared with free drug (45.04 \pm 8.12 %) over the entire experimental duration, confirming their excellent mucoadhesive properties.

2.9. In vivo pharmacokinetics and biosafety of GelMAP nanosuspension

We assessed the *in vivo* ocular pharmacokinetics of MFX-loaded GelMAP nanosuspension (0.5 % (w/v)) in comparison to commercial MFX eye drops, Vigamox® (0.5 % (w/v)), using healthy mice. Each mouse received a topical instillation of either MFX-loaded GelMAP nanosuspension or Vigamox® (MFX ophthalmic solution). At designated time points up to 48 h post-dosing, corneas and aqueous humor were collected from euthanized mice (n = 4–5 per group per time point). Drug concentrations in these samples were quantified using high-performance liquid chromatography (HPLC), and key pharmacokinetic parameters

were determined, including C_{max} (maximum drug concentration), T_{max} (time to reach C_{max}), $T_{1/2}$ (half-life, indicating how long the drug remains in the system), and $AUC_{0.24h}$ (area under the concentration-time curve over 24 h, representing overall drug exposure). These parameters

provide insights into drug absorption, retention, and clearance in ocular tissues.

Our results showed that eyes treated with MFX-loaded GelMAP nanosuspension obtained higher concentrations of MFX in both the

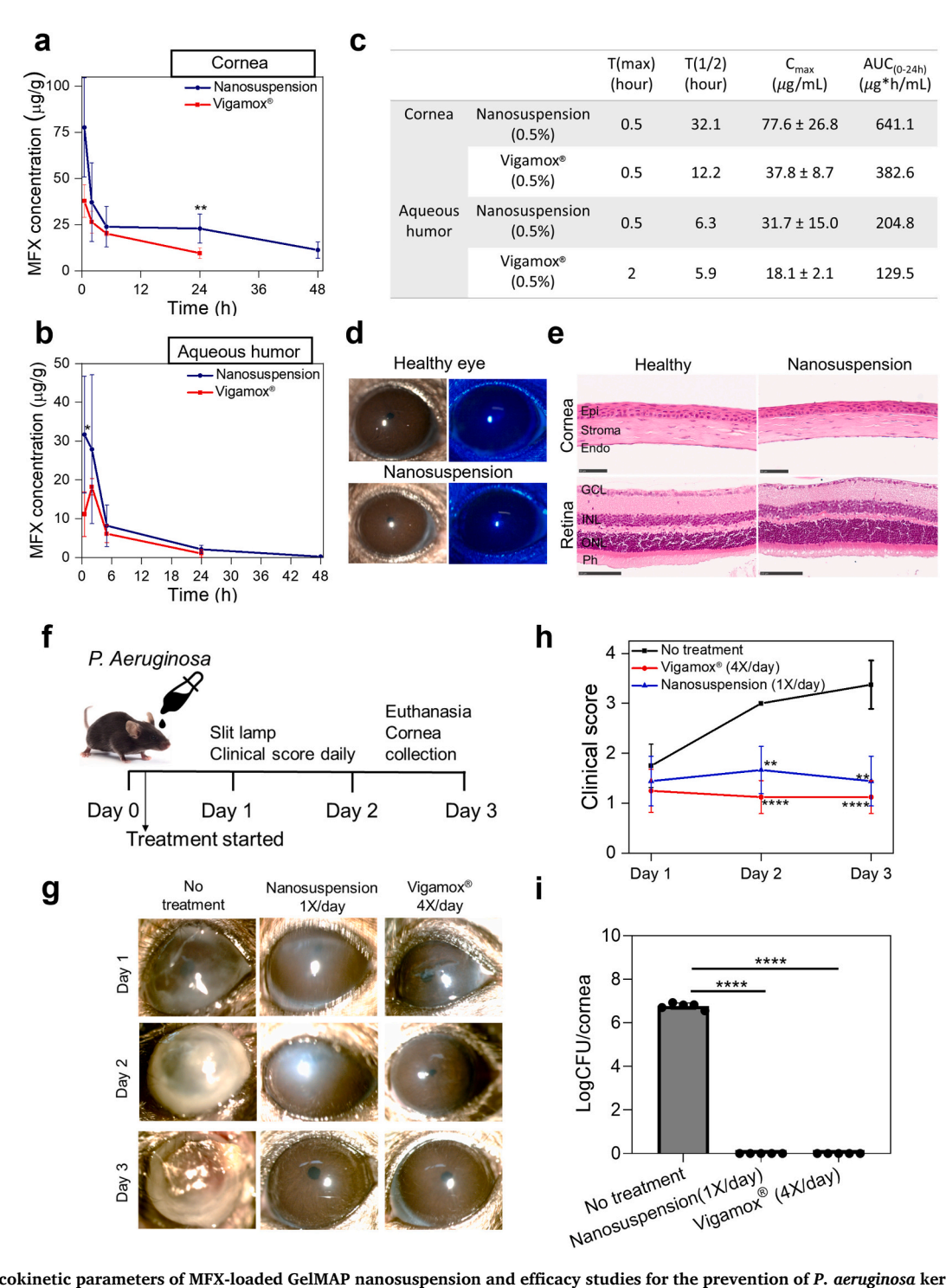


Fig. 5. Pharmacokinetic parameters of MFX-loaded GelMAP nanosuspension and efficacy studies for the prevention of P. aeruginosa keratitis in a murine model. Drug concentration-time curve in (a) cornea and (b) aqueous humor in mice. (c) C_{max} and AUC_{0-24h} values of MFX-loaded GelMAP nanosuspension (0.5 % MFX) in the cornea and aqueous humor compared to 0.5 % commercial Vigamox® (n=4-6). Statistical significance was determined using an unpaired, two-tailed Student's t-test. (d) Slit lamp bright field and Cobalt blue light images of corneas of healthy mice before and after 7-day topical treatment with GelMAP nanosuspension. (e) Histological analysis of the eye demonstrated an intact corneal and retinal morphology on day 7 (scale bars; cornea: 50 μ m, retina: 100 μ m). Corneal epithelium (Epi), stromal tissue, and endothelial tissue (Endo); Photoreceptor layer (Ph), Outer Nuclear Layer (ONL), Inner Nuclear Layer (INL) and Ganglion Cell Layer (GCL). The healthy cornea (normal) serves as a control. (f) Schematic of study design; (g) slit lamp photos; (h) clinical score and (i) bacterial counts (CFU/cornea) on day 3. Error bars indicate the standard deviation of the means, asterisks mark significance levels of p < 0.05 (*), p < 0.01 (**), and p < 0.0001 (****), ns = not significant, n = 5-9 (Kruskal-Wallis test or one-way ANOVA). (For interpretation of the references to color in this figure legend, the reader is referred to the web version of this article.)

cornea (Fig. 5a) and aqueous humor (Fig. 5b) over 24 h compared to the Vigamox\$. In the cornea, the C_{max} at 0.5 h and the $AUC_{0.24h}$ in the MFX-loaded GelMAP nanosuspension group were 2.05 times and 1.68 times greater than the values achieved with Vigamox\$, respectively (Fig. 5c). The antibacterial efficacy of the fluoroquinolones, including MFX, is

closely associated with the ratio of AUC to the minimum inhibitory concentration (MIC) [89]. Therefore, the higher AUC for the MFX-loaded GelMAP nanosuspension reflects its enhanced bioavailability and potentially superior antibacterial efficacy. Additionally, the $T_{1/2}$ of the drug delivered by MFX-loaded GelMAP nanosuspension was 2.63

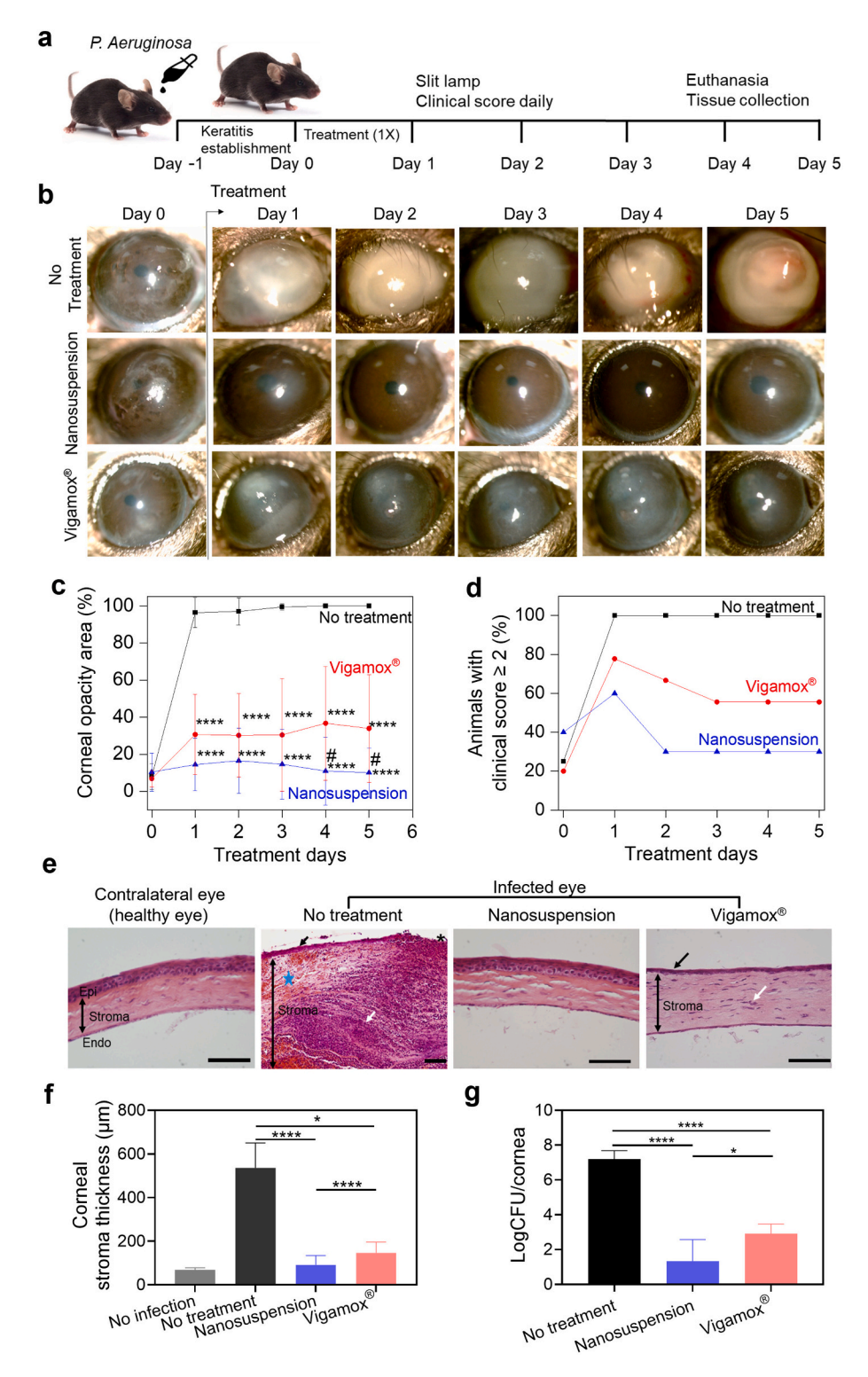


Fig. 6. *In vivo* efficacy studies of MFX-loaded GelMAP nanosuspension in a murine model of *P. aeruginosa* keratitis. (a) Schematic representation of the study design; (b) slit lamp photographs; (c) quantification of the opacity area (**** compared to no treatment; # compared to Vigamox®); (d) percentage of animals with a clinical score of ≥ 2 ; (e) representative H&E stained images (scale bar: 200 μ m); (f) measurements of corneal stromal thickness (μ m) following different treatments and (g) bacterial counts (CFU per cornea) at the endpoint. Error bars represent the standard deviation. Asterisks denote the significance levels of p < 0.05 (* or #), p < 0.0001 (****), ns = not significant. Sample size (n) is ≥ 3 (One-way ANOVA).

times longer than that provided by the Vigamox®, indicating significantly improved drug retention on the ocular surface (Fig. 5c). In the aqueous humor, the MFX-loaded GelMAP nanosuspension group exhibited C_{max} and $AUC_{0.24h}$ values that were 1.75-fold and 1.58-fold higher, respectively, than those of the commercial Vigamox® eye drops. These findings suggest that MFX-loaded GelMAP nanosuspension offers superior ocular penetration and extended retention, improving ocular bioavailability compared to commercial formulations.

We conducted a further evaluation of the safety of GelMAP nanosuspension. Mice were administered the nanosuspension daily for 7 days and their eyes were monitored daily for signs of tearing, discharge, or any other symptoms indicative of ocular discomfort or infection. Highresolution assessments of the corneas and ocular surface were performed using a slit-lamp biomicroscope, with photographs taken on days 0, 1, 2, 4, and 7 (Fig. S13). Additionally, fluorescein staining was performed on 7 days to assess any epithelial defects, and hematoxylin and eosin (H&E) staining was conducted on the eyes 7 days after treatment. Untreated normal mice served as controls. Throughout the study, no adverse effects and epithelial defects were observed (Fig. 5d). The cornea and retina in the GelMAP nanosuspension group showed no detectable differences compared to normal eyes. The result of H&E staining showed no notable loss of corneal epithelium (Epi), stromal tissue, or endothelial tissue (Endo), nor any signs ofinflammatory cell infiltration (Fig. 5e). The retinal structure in the GelMAP nanosuspension group also appeared normal, showing intact histological layers, including the photoreceptor layer (Ph), outer nuclear layer (ONL), inner nuclear layer (INL), and ganglion cell layer (GCL) (Fig. 5e). These results confirm the in vivo safety of the GelMAP nanosuspension. While these findings support the short-term biosafety (7 days) of the formulation, we acknowledge that long-term safety, particularly under repeated or chronic administration, remains to be investigated. Future studies will focus on extended in vivo evaluations to assess the potential for cumulative toxicity and ensure suitability for long-term clinical use.

2.10. In vivo evaluation of prophylactic and therapeutic efficacy of GelMAP nanosuspension

To test whether the superior ocular pharmacokinetics of MFX-loaded GelMAP nanosuspension translated into greater treatment effectiveness, we tested the antimicrobial efficacy of MFX-loaded GelMAP nanosuspension in an *in vivo* murine bacterial keratitis model using *P. aeruginosa* (ATCC 19660). We assessed efficacy under two stages: (1) Onset, to evaluate prophylactic effectiveness (Figs. 5f-i) by administering the nanosuspension immediately after bacterial inoculation to prevent infection before it develops, and (2) Established, to assess treatment efficacy by applying the nanosuspension after a one-day incubation period, simulating a delayed intervention scenario (Fig. 6).

To study the prophylactic efficacy [90] (Fig. 5f), the mice were randomly assigned to one of three groups: 1) no treatment; 2) Vigamox® $(4\times/day)$; and 3) MFX-loaded GelMAP nanosuspension $(1\times/day)$. The corneal opacity area and clinical scores were accessed by analysis of slit lamp photos. An established scoring system with a grading scale ranging from 0 to 4 was then employed to assess the disease severity [90]. A score of 0 denotes normal findings, and higher grades indicate a progressively more severe infection. After treatment, corneas were harvested for bacterial enumeration and histopathological analysis. Corneas with no treatment exhibited severe opacity (Fig. 5g), high clinical score (Fig. 5h), and high bacterial counts within 3 days (Fig. 5i). In contrast, corneas treated with Vigamox® or MFX-loaded GelMAP nanosuspension showed clear cornea (Fig. 5g) and lower clinical score after 3-day treatment (Fig. 5h). Bacterial count data in the prophylactic study showed that either commercial MFX drops (4×/day) or our MFXloaded GelMAP nanosuspension formulation (1×/day) completely sterilized the infected eyes after 3-day treatment (Fig. 5i). These findings emphasized the comparable efficacy of MFX-loaded GelMAP nanosuspension (1×/day) to the commercial Vigamox® eye drops (4×/day)

in the prevention of bacterial keratitis in mice.

We further evaluated the treatment efficacy under more severe, late-stage ocular infection conditions to assess the performance of the nanosuspension. Keratitis was initially established by topically administering *P. aeruginosa* (1000 colony-forming unit (CFU) /cornea) to an injured cornea, followed by a one-day incubation (Fig. 6a) [91]. The mice were randomly assigned to one of three groups: 1) no treatment; 2) MFX-loaded GelMAP nanosuspension, applied only on day 0 over 5 days; 3) commercial Vigamox® drops, administered only on day 0 over 5 days. Corneal disease progression was monitored daily *via* slit-lamp examination, and infection severity was graded (0–4) by a masked ophthalmologist using a standardized scoring system based on slit-lamp images [90]. The corneal opacity area was quantified from slit-lamp images using ImageJ software. After treatment, corneas were harvested for bacterial enumeration and histopathological analysis.

Slit-lamp assessment (Figs. 6b-d) showed that following a one-day inoculum incubation, mice across all groups displayed comparable disease severity on day 0, with an average corneal opacity area of approximately 8.5 % (Fig. 6c), confirming the consistent establishment of P. aeruginosa keratitis. In the no treatment group, the disease progressed rapidly, with pronounced corneal opacity observed after day 1 (Figs. 6b and c). All untreated eyes had clinical scores of >2 by day 1, indicating severe infections that were challenging to treat. By day 3, 20 % (2/8) of the eyes had corneal perforation (clinical score of 4, humane endpoint), which increased to 37.5 % (3/8) by day 4 and 62.5 % (5/8) by day 5 (Fig. 6d). In contrast, the MFX-loaded GelMAP nanosuspension or Vigamox® treatment resulted in significantly lower ocular opacity area (Figs. 6b and c) and clinical scores from days 1 to 5 compared to the no-treatment group (Fig. 6d, p < 0.001). In addition, the MFX-loaded GelMAP nanosuspension group exhibited less ocular opacity compared to the Vigamox® group from days 1 to 5 (Figs. 6b and c), with statistical significance observed on days 4 and 5 (Fig. 6c, p < 0.05), indicating a clear benefit associated with the nanosuspension treatment. By day 5, a concerning 56 % of the eyes treated with Vigamox® drops exhibited clinical scores of 2 or higher. In contrast, only 30 % of the eyes in the MFX-loaded GelMAP nanosuspension group displayed similar scores (Fig. 6d), highlighting the effectiveness of the GelMAP nanosuspension. In the late-stage keratitis model, clinical corneal opacity areas were comparable between the Vigamox® and MFX-loaded GelMAP nanosuspension groups during the early treatment phase (days 1–3; Fig. 6c), likely due to the high baseline inflammation present at the onset of treatment, which persisted despite initial bacterial reduction. Although Vigamox® initially reduced bacterial load, its rapid clearance from the ocular surface limited sustained therapeutic exposure. In contrast, the MFX-loaded GelMAP nanosuspension enabled prolonged ocular retention and sustained drug release, supporting continued antimicrobial and anti-inflammatory activity. This sustained effect became more evident in the later treatment stages, resulting in significantly improved outcomes by days 4-5. These findings underscore the importance of long-acting delivery systems in achieving superior therapeutic efficacy for established ocular infections.

To assess disease progression further, histological analysis was conducted on the eyes 5 days after treatment (Figs. 6e-g). The contralateral eye (no infection) served as a control. H&E staining of the contralateral eye's cornea revealed a relatively uniform epithelial layer consisting of 5–7 cell layers, a stroma layer consisting of parallel arranged collagen bundles with normal stromal thickness (69.1 \pm 9.1 μ m) (Fig. 6e), and an intact endothelium layer. In the no-treatment group, H&E staining revealed significant damage by showing reduced corneal epithelium cell layers (2–3 cell layers, black arrow), complete loss of corneal epithelium layer (marked black *) in some regions, severe stromal thickening (536.0 \pm 114.2 μ m, indicative of severe edema), extensive inflammatory cell infiltration (white arrow), disrupted collagen fibers in stroma (blue star), and corneal perforation, all pointing to severe inflammation. Infected eyes treated with commercial Vigamox® drops retained the three corneal layers but exhibited partial epithelial loss (2–3 layers,

black arrow) in some regions, moderate stromal thickening (146.7 \pm 49.7 $\mu m)$, and some inflammatory cell infiltration in the stroma (white arrow), indicating a moderate inflammatory response. In contrast, corneas treated with MFX-loaded GelMAP nanosuspension showed minimal inflammatory cell presence, with stromal thicknesses and epithelial cell layers closely resembling the normal corneal structure (Figs. 6e-f).

Viable bacterial plate counts were assessed in the corneas (n=5 per group) at the endpoint of the study. Both MFX-loaded GelMAP nanosuspension and Vigamox® eye drops resulted in a significant reduction in bacterial counts, demonstrating more than a 3-log decrease in CFU compared to the no treatment group (Fig. 6g). Notably, the corneas treated with MFX-loaded GelMAP nanosuspension had a significantly lower number of viable bacteria (p < 0.05) compared to those treated with the commercial Vigamox® (Fig. 6g). These findings emphasized the superior efficacy of MFX-loaded GelMAP nanosuspesion over the commercial MFX eye drops for the treatment of P. aeruginosa keratitis, aligning with the results observed in pharmacokinetic studies (Fig. 5a-c).

Our goal in this study was not to determine the optimal clinical dosing regimen, nor to propose a therapeutic protocol, but rather to evaluate the efficacy of the MFX-loaded GelMAP nanosuspension under controlled experimental conditions. To this end, we compared the dropto-drop efficacy of our formulation with the standard of care, Vigamox®. In the prophylactic model, where a virulent bacterial strain was used, our aim was to maintain a sterile corneal surface and prevent infection. Vigamox® was administered four times daily following its clinical usage, while GelMAP was given once daily. Despite the reduced dosing frequency, the once-daily GelMAP treatment showed comparable prophylactic efficacy to Vigamox®, highlighting the benefit of sustained release. After confirming this equivalence, we proceeded to evaluate therapeutic efficacy in an established infection model, in which treatment was initiated after allowing infection to develop. In this model, both groups received a single drop of eyedrops on Day 0, allowing a direct, head-to-head comparison. Under these matched conditions, the MFX-loaded GelMAP nanosuspension demonstrated superior therapeutic efficacy compared to Vigamox®. While these results support the promise of our nanosuspension as a sustained-release alternative, we emphasize that determining the preferred or optimal clinical dosing regimen will require further investigation in future translational studies.

The engineered MFX-loaded GelMAP nanosuspension demonstrated robust prophylactic and therapeutic efficacy, offering a dual-function strategy that addresses bacterial ocular infections at multiple stages. This platform not only prevents infection onset but also effectively treats established disease, reducing the need for frequent administration and improving treatment outcomes. By integrating prevention and treatment into a single, sustained-release system, GelMAP has the potential to simplify ocular care, lower the risk of complications, and significantly improve patient compliance. Currently, no NP formulations have demonstrated this dual efficacy in managing both the onset and established conditions of ocular infections, highlighting the potential of MFXloaded GelMAP nanosuspension. Specifically, it may be effective in preventing infections following ocular surgeries or injuries, such as cataract surgery-associated endophthalmitis. Additionally, MFX-loaded GelMAP nanosuspension may serve as a treatment for existing ocular conditions like bacterial keratitis or conjunctivitis. Most existing NPbased therapies for ocular infections have been shown to be effective within short time frames (typically less than 48 h) [92-94]. While some studies have reported prolonged antibacterial effects [95-97], these formulations lack in vivo comparisons with commercial eye drops, making it difficult to assess their clinical relevance and translational potential. MFX-loaded GelMAP nanosuspension, therefore, represents a significant advancement in ocular infection management, combining preventive and therapeutic benefits in a single, long-lasting solution.

3. Conclusion

We sought to address the currently unmet clinical need in the development of a mucoadhesive nanosuspension that can significantly improve the bioavailability of drugs and patient compliance by reducing the frequency of dosage. Biocompatible GelMA NPs were functionalized with a PBA targeting moiety to endow the NPs with mucoadhesiveness for prolonged delivery of the loaded MFX. The drug-loaded NPs were then dispersed in a matrix optimized with proper viscosity, mucoadhesion, lubrication, and most importantly, shear-thinning properties. The engineered nanosuspension demonstrated sustained release of the drug and was effective in killing bacteria over a significantly longer period as compared with free MFX. The mucoadhesion of the prepared GelMAP nanosuspension was thoroughly evaluated in vitro by zeta potential assessments, turbidity tests, fluorescent methods, PAS staining assays, and an ex vivo set up using fresh pig eyeballs. In addition, in vitro biocompatibility tests ensured its safe utility in biomedical field. Finally, our in vivo studies demonstrated the strong potential of GelMAP nanosuspension for successful clinical translation in treating both early- and late-stage ocular infections, outperforming commercial eye drops. We believe the designed nanosuspension, featured with a high level of biocompatibility and bioavailability, ease of use, and strong mucoadhesion, has the potential to find wide applications in emergency healthcare and a variety of complex ocular complications.

4. Materials and methods

4.1. Materials

Gelatin from porcine skin (Bloom 300, type A), methacrylic anhydride 94 %, 3-amino phenyboronic acid, glutaraldehyde solution (70 %), 2-hydroxy-4'-(2-hydroxyethoxy)-2-methylpropiophenone, porcine gastric mucin, were all purchased from Sigma-Aldrich. Moxifloxacin hydrochloride was obtained from TCI chemicals. 1-(3-Dimethylaminopropyl)-3-ethylcarbodiimide hydrochloride (EDC), ysuccinimide (NHS), and 3-aminophenylboronic acid (PBA) were obtained from TCI chemicals. Dulbecco's phosphate buffered saline (DPBS) was purchased from GE Healthcare Life Sciences. Other chemicals and organic solvents used in this study were purchased from Sigma-Aldrich and used as received unless stated otherwise. Staphylococcus aureus (S. aureus) and Pseudomonas aeruginosa (P. aeruginosa) were obtained from ATCC.

4.2. Synthesis of GelMA

GelMA was synthesized based on a previously developed protocol [98]. Briefly, 10 % (w/v) of gelatin was dissolved in DPBS solution and reacted with 8 % (v/v) of methacrylic anhydride at 60 °C for 3–4 h. After the methacrylate reaction stopped, the solution was then filled in dialysis membranes (10 k \sim 12 k MW) and dialyzed for 5 days with Milli Q water replaced twice per day to remove excess methacrylic anhydride remaining. The solution was then filtered and transferred into falcon tubes and freeze-dried at $-80~^{\circ}\text{C}$ for 5 days. ^{1}H NMR was performed to verify $\sim\!80~\%$ meth-acryloyl functionalization degree.

4.3. Synthesis of GelMAP prepolymer

To functionalize GelMA with PBA, 2.25 % (w/v) GelMA was dissolved in 0.1 M 2-(N-morpholino) ethane sulfonic acid (MES) at pH = 5.5–6, stirring at 45 °C. Next,EDC andNHS were added to activate the carboxyl group of GelMA and the reaction was left to stir for \sim 1 h at 45 °C. Then,PBA was added to the solution, and the pH of the solution was adjusted to 6 by adding 1 M NaOH and letting it react for 12 h at 25 °C to yield GelMAP. The synthesized GelMAP was dialyzed against water to remove unreacted EDC/NHS. 1 H NMR was performed to verify the successful conjugation of PBA to GelMA. The molar ratio of COOH

(from GelMA): EDC: NHS: PBA was fixed at 1:5:10:5.

4.4. ¹H nuclear magnetic resonance (¹H NMR) characterization

DMSO- d_6 (10 mg/mL) was used to dissolve gelatin, GelMA, GelMAP and PBA. 1 H NMR spectra were recorded by applying 10 s recycle delay for 64 scans at ambient temperature using a Bruker DRX 400 spectrometer working at 400 MHz. Conjugation efficiency of PBA to GelMA was determined by 1 H NMR in D₂O. The aromatic protons of PBA (7.5–7.8 ppm) were integrated relative to the alanine methyl peak (\sim 1.4 ppm). Based on known amino acid composition and manufacturer-reported molecular weight and carboxyl content.

4.5. Synthesis of GelMAP NPs

GelMA and GelMAP NPs were prepared using a desolvation technique previously reported by Kimura et al. [99] with some modifications. Briefly, 100 mg of GelMA or GelMAP was dissolved in 2 mL of deionized (DI) water at 45 °C under constant stirring (660 rpm). After the complete dissolution of biopolymers, the pH was adjusted to 7.4–7.5 at room temperature using 0.1 M NaOH or HCl. Next, ~3 mL of acetone was added dropwise into the solution at 45 °C under constant stirring (660 rpm) until a faint permanent turbidity was observed. 2 µL of glutaraldehyde (GA) and 55 µL of Irgacure 2959 solution (from a freshly prepared stock solution of 11 mg/mL) were pipetted into the solution, respectively. The solution was stirred at 45–50 °C for 2–3 h at 600 rpm, followed by UV crosslinking for 20 min for NPs stabilization. Then, the mixture was left to stir further for 2-3 h. The acetone fraction in the solution was then evaporated using a rotary evaporator, and the concentration of MFX after rotary evaporation was determined using a UV-vis spectrophotometer and could be controlled by evaporation time. The solution containing GelMA or GelMAP NPs was collected in a glass vial and stored at 4 °C for further characterization.

4.6. Matrix formulation and characterization

The matrix was made of active ingredients: HA (0.1-0.5 %, (w/v)), glycerin (0.3 %–1 %, (w/v)), hypromellose (0.3 %, (w/v)) and inactive ingredients: boric acid (0.8 %, (w/v)) calcium chloride (0.0053 %, (w/ $\!\!\!$ v)) magnesium chloride (0.0065 %, (w/v)), benzalkonium chloride (0.0065 %, (w/v)), potassium chloride (0.038 %, (w/v)), sodium chloride (0.4 %, (w/v)), zinc chloride (0.00015 %, (w/v)). The pH of the final mixture was adjusted to 7.4. The rheological properties of the blank matrix and the matrix mixed with MFX-loaded GelMAP NPs were characterized using a Modular Compact Rheometer MCR302. The results were obtained by linking the measuring system PP08 with a diameter of 8 mm to the rheometer. Each measurement was carried out by loading a fresh sample in the 1 mm gap between the parallel plates and removing excessive samples. At a given shear rate parameter, ranging from 1 to 1000 s⁻¹ with 30 measuring points, the relationship of viscosity and shear stress as a function of shear rate was recorded. The wettability of the matrix was characterized on the mucin-coated slides with the wetting area measured by a caliper. Oscillatory rheological measurements were conducted using a Modular Compact Rheometer MCR302 equipped with a PP08 parallel plate geometry at 37 °C. A frequency sweep was performed over the range of 1-20 rad/s at a constant strain of 1 %, which was confirmed to be within the linear viscoelastic region based on preliminary strain sweep tests. The storage modulus (G') and loss modulus (G") were recorded to assess the viscoelastic properties of the blank matrix and the MFX-loaded GelMAP nanosuspension.

4.7. Transmission electron microscopy (TEM) analysis

A 4 μL of GelMAP NPs solution with 10 times dilution in Milli-Q water was added onto a TEM grid (Electron Microscopy Sciences,

Formvar/Carbon 200 Mesh, Copper), dried overnight and imaged using a T12 Quick room temperature TEM with 120 kV electron-beam energy.

4.8. Particle size, PDI and zeta potential characterization of empty and MFX loaded GelMAP NPs

The hydrodynamic size and PDI of GelMA or GelMAP NPs were characterized using a Malvern Panalytical DLS Zetasizer. The bulk suspension of NPs was diluted in Milli-Q H_2O (10 μL of emulsions in 1 mL of Milli-Q H_2O) in a disposable folded capillary cell (DTS1070). The zeta potential was also determined by using a disposable folded capillary cell (DTS1070) on the same instrument, with three measurements taken per sample following standard operating procedures.

4.9. Encapsulation efficiency characterization

The encapsulation efficiency of MFX loaded GelMAP NPs was determined by diluting the filtrate (after passing through a 10 K membrane) of the MFX loaded GelMAP NPs dispersion with DI water and measuring spectrophotometrically the absorbance at 292 nm using a Thermo Scientific NanoDrop Moreone Microvolume UV-vis spectrophotometer. Standard samples were made by preparing a serial dilution of MFX solution from the MFX stock solution (35 mg/mL) in DI water.

Then the filtrate absorbance for each batch of MFX loaded GelMAP NPs was analyzed using a calibration curve and re-calculated for the encapsulated concentration using Eq.1

$$\mbox{Encapsulation Efficiency (\%)} = \frac{C_{total} - C_{free}}{C_{total}} \times 100 \eqno(1)$$

 C_{total} is defined as the total amount of MFX added and C_{free} is the amount of free MFX measured inside the filtrate. The value of $C_{total}-C_{free}$ equals to the drug concentration loaded inside the MFX loaded GelMAP NPs.

4.10. In vitro release study

The *in vitro* release profiles of MFX from GelMAP NPs were determined by a dialysis method as described previously [31]. Briefly, 0.2 mL of MFX-loaded GelMAP NPs or free MFX was mixed with 0.2 mL matrix, and the mixture was transferred into dialysis membranes (molecular weight cut-off: 10–12 kDa) and submerged into artificial tear fluid (10 mL total volume) inside glass vials. At predetermined time points, 1 mL of sample was taken and replaced with fresh 1 mL of artificial tear for up to 6 days. The amount of MFX released at each time point was analyzed using a Thermo ScientificTM NanoDropTM One/OneC microvolume UV–vis spectrophotometer. The composition of artificial tear fluid used was sodium chloride 0.670 g, sodium bicarbonate 0.200 g, calcium chloride· $2H_2O$ 0.008 g, purified water 100.0 g [100].

4.11. In vitro mucoadhesion characterizations

4.11.1. Zeta potential assessment

Zeta potential assessment of the NPs was performed as described previously [31]. Briefly, commercially available porcine gastric mucin was made into a 1 mg/mL solution with deionized water and the solution was placed overnight. 1 mL of GelMAP or GelMA NPs solutions of different concentrations (0.03125, 0.0625, 0.125, 0.25, 0.5, 1 %, (w/v)) were mixed with 1 mL of mucin solution and the mixed solution was shaken at 37 $^{\circ}\mathrm{C}$ for 1 h. The zeta potential of the mixed solution was measured using a Malvern Panalytical DLS Zetasizer.

4.11.2. Hydrodynamic size measurement

 $0.5\,\%$ GelMA or GelMAP NPs were mixed with 0.05 % mucin for 1 h at 37 $^{\circ}\text{C}.$ Hydrodynamic size measurements were performed on the mixture afterwards using a Malvern Panalytical DLS Zetasizer.

4.11.3. Sialic acid -targeting evaluation via fluorescence method

The suitable excitation wavelength and the emission wavelength range were first determined by a spectrofluorometer (Photon Technologies International QuantaMaster) using 1 % (w/v) GelMAP NPs solution. Then, 1 % GelMAP or GelMA NPs were mixed with varying concentrations of SA solutions (0, 0.01, 0.02, 0.03, 0.05, 0.1, 0.2, 0.3 mM). The mixtures were vortexed for 30 s before measurement with a plate-reader-type spectrofluorometer (Tecan Infinite M1000 Pro). The samples were excited at 295 nm, and an emission scan from 335 to 435 nm was obtained for each sample.

4.11.4. Turbidity assay

The mucoadhesive properties of GelMAP NPs were evaluated by transmittance analysis. 10 μ L of GelMA or GelMAP NPs (5 %, (w/v)) were added into 1 mL of mucin solution (dissolved in DPBS) at different concentrations (0.25 %, 0.5 %, 1 %, (w/v)), followed by 30 s of vigorous vortexing. Afterward, sample transmittance was measured at 600 nm. DPBS was analyzed as a control.

4.11.5. Atomic force microscopy (AFM) analysis

100 μ L of mucin (0.1 %, (w/v)) was spin-coated (1000 RPM, 1 min) on Muscovite Mica (Electron Microscopy Sciences, US). 100 μ L of GelMA or GelMAP NPs (5 %, (w/v)) were spin-coated (1000 RPM, 1 min) on top of the mucin-coated mica for 1 h. The absorbed surface was then washed three times using Milli-Q H₂O, followed by overnight drying in the desiccator. All imaging was performed in the air in the fast scanned mode (Bruker Dimension®FastScan® Atomic Force Microscope with ScanAsystTM) at a scan rate of 0.901 Hz with a 5 μ m scan size. All measurements of the images, such as mean roughness (Ra) were performed using the Nanoscope Analysis software provided by the Bruker FastScan AFM.

4.11.6. Periodic Acid-Schiff (PAS) Staining

PAS staining was performed based on a previous protocol [38]. Briefly, NPs were suspended in 1 mL of 1 mg/mL mucin solution (in DPBS), and the solution was incubated at 37 °C for 1 h. Then the suspension was centrifuged at 8000 rpm for 30 min, and the free mucin in the supernatant was determined by PAS staining. The supernatant was mixed with 200 μ L periodic acid reagent and incubated at 37 °C for 2 h; then it was added to 200 μ L Schiff reagent and incubated for 30 min at room temperature. The absorbance was determined at 555 nm. The amount of mucin adsorbed onto NPs was measured by subtracting the amount of free mucin from the initial mucin amount.

4.12. In vitro antibacterial characterizations

MFX-loaded GelMAP NPs or free MFX (used as a positive control) were first dispersed in the matrix (1.2 % (w/v)) and were put into dialysis bags (10-12 k MW). Two strains of bacteria, P. aeruginosa and MRSA, were used to evaluate the long-term antibacterial effects of the MFX-loaded GelMAP NPs. The dialysis bags (10 k \sim 12 k MW) were put into the bacteria solution (OD 0.07-0.09, 3 mL) to allow drug release and every 24 h, the dialysis bags were taken out from the bacteria solution. The turbidity (OD = 625 nm) of the bacteria solution was determined to evaluate the antibacterial effects. Meanwhile, the dialysis bags were immediately put into fresh bacteria solution to further assess the long-term killing effects of the NPs. The antibacterial effects were evaluated for 7 days with turbidity measured every day. On days 1, 4, and 7, 0.1 mL of bacterial solution was taken from each incubated sample and diluted with broth to a 3-log range. Then, 100 μL of the solution was added to each agar plate and uniformly spread over it for colony visualization.

4.13. In vitro biocompatibility test

The cytocompatibility of the engineered GelMAP NPs and matrix was

first evaluated separately through in vitro viability and metabolic activity of NIH 3T3 fibroblasts. Commercial Live/Dead kits (Invitrogen) and Actin/(4',6-diamidino-2-phenylindole) DAPI staining (Invitrogen) were used to evaluate cell viability and proliferation, respectively. A Prestoblue assay (Life Sciences) was performed to assess the metabolic activity of the cells. NIH 3T3 cells were seeded on the bottom of a 48well at a cell density of 2×10^4 cells/well. 300 µL of growth medium (Dulbecco's Modified Eagle's Medium) was added to each well with 30 μL or 50 uL GelMAP NPs (5 %, (w/v)), 10 μL matrix directly added into it. The well plates were sustained at 37 °C in a humidified atmosphere containing 5% CO2 for 5 days with the culture medium and GelMAP NPs being replaced every 48 h. The viability of 3T3 cells grown on the bottom of well plates was evaluated using a Live/Dead viability kit according to manufacturer instructions (n = 4). In brief, cells were stained with 0.5 μ L/mL of calcein AM and 2 μ L/mL of ethidium homodimer-1 (EthD-1) in DPBS for 20 min at 37 °C. On the first- and fifth-day postseeding, fluorescent imaging was performed using an AxioObserver Z7 inverted microscope. Viable and dead cells were visualized by their green and red color, respectively; and quantified using ImageJ software. Cell viability was determined as the number of live cells divided by the total number of cells. The metabolic activity of the cells was assessed on the first- and fifth-day post-seeding using a PrestoBlue assay (Life Technologies) (n = 6). The 3 T3 cells were incubated in 200 μ L of 10 % (v/v) PrestoBlue reagent in a growth medium for 45 min at 37 °C. Fluorescence was measured using a Synergy HT fluorescence plate reader (BioTek).

F-actin and cell nuclei staining were used to visualize the spreading of 3T3 cells at the bottom of the 48-well plates (n = 4). Cells at days 1 and 5 post-seeding were fixed in 4 % (v/v) paraformaldehyde (Sigma) for 15 min, permeabilized in 0.1 % (w/v) Triton X-100 (Sigma) for 5 min, and blocked in 1 % (w/v) bovine serum albumin (BSA, Sigma) for 30 min. Afterward, samples were incubated with Alexa fluor 488 phalloidin for 45 min. Following repeated washes with DPBS, samples were counterstained with 1 $\mu L/mL$ of DAPI in DPBS for 2 min and fluorescent imaging was completed using an inverted fluorescence microscope (Zeiss Axio Observer Z7). Following the validation of biocompatibility on 3T3 cells, HCE cells were subsequently used to assess the biocompatibility of the GelMAP NPs combined with the matrix. A mixture of 10 μL of NPs and 10 μL of matrix was prepared, and the evaluation was performed using previously described methods. The HCE cells were cultured in Alveolar Epithelial Cell Medium, obtained from ScienCell Research Laboratories.

4.14. Ex vivo retention characterizations

Pig eyeballs were freshly harvested and used immediately followed by euthanasia. To better visualize the prolonged retention effects, Gel-MAP NPs (5 % (w/v)) were first loaded with a hydrophilic red dye, Rhodamine B using the same method, and then applied to the eyeballs (200 μL). GelMA NPs (5 % (w/v)) loaded with Rhodamine B served as a control. After incubation for 30 min, eyeballs were immersed in artificial tear fluid to let the NPs detach from the ocular surface. At each predetermined time point, the absorbance at 550 nm, a wavelength corresponding to Rhodamine B, was recorded to evaluate the retention effects of the GelMAP NPs using a Thermo Scientific Nano Drop One One microvolume UV–vis spectrophotometer.

For the drug retention study, nanosuspension and a free drug solution (in matrix) were prepared. The eyeballs of the pigs were taken out and immediately treated with drops of the prepared solutions (200 μL), followed by incubation for 15 min based on a previously developed protocol [31]. The eyeballs were washed vertically with artificial tear at a rate of 0.5 mL/min. The washing solution was collected at 10, 30, 60, 120 and 180 min, respectively. The content of MFX in the washing solution was quantified using a Thermo Scientific NanoDrop One/OneC microvolume UV–vis spectrophotometer at 292 nm.

4.15. Animals and in vivo biocompatibility

Male and female C57BL/6 mice, aged 8–10 weeks, were obtained from Charles River Laboratories in Wilmington, MA. All experiments conducted for this study received approval from the Schepens Eye Research Institute Animal Care and Use Committee (animal protocol number: 2021N000158). The treatment of all animals adhered to the ARVO Statement for the Use of Animals in Ophthalmic and Vision Research. Prior to all surgical procedures, each animal was deeply anesthetized with an intramuscular injection of 3 to 4 mg of ketamine and 0.1 mg of xylazine.

The eyes of healthy mice (n=3) were treated with one drop of GelMAP nanosuspension daily for 7 days and monitored for signs of tearing, discharge, or other symptoms indicative of ocular discomfort or infection. Observations were documented daily, with photographs taken on days 0, 1, 2, 4, and 7 using a slit-lamp biomicroscope. Additionally, to assess any epithelial defects, 1 μ L of 2.5 % fluorescein (Sigma-Aldrich) was applied to the lateral conjunctival sac of unanesthetized mice with a micropipette; the eyes were examined after 3 min for fluorescein staining using a slit lamp biomicroscopy under a cobalt blue light on day 7. Normal (untreated) mice served as controls. On day 7, all mice were euthanized, and their eyes were harvested for histopathological analysis.

4.16. Ocular pharmacokinetics in mice

In the pharmacokinetic study, both eyes of the healthy mice received one drop ($\sim 5~\mu L$) of either MFX commercial eye drops or MFX-loaded GelMAP nanosuspension. After the drops were administered, the mice (n=4--5 mice per time point per group) were euthanized at predetermined time points (0.5 h, 2 h, 5 h, 24 h, or 48 h). Right after the euthanasia, aqueous humor ($\sim 5~\mu L$) and corneal tissue ($\sim 5~mg$) from both eyes were collected and stored at $-80~^{\circ} C$. The different mice were re-dosed with eye drops at each time point. Drug concentrations in the tissues were quantified using HPLC with fluorescence detection (Dionex^TM ICS 5000 + system, Thermo Fisher Scientific). The measured MFX concentration was further plotted against time. The C_{max} and time to reach C_{max} (t_{max}) after dosing were recorded as observed. The AUC(0–24h) for each group was calculated using linear trapezoid rules [101].

4.17. Bacterial strains and inoculum preparation

The *P. aeruginosa* ATCC strain 19660, commonly used as a standard laboratory strain, was utilized in this study because it consistently produces corneal pathology in the C57BL/6 mouse model. The frozen stock of *P. aeruginosa* was cultured on 5 % sheep blood agar plates at 37 °C. After 18 h of incubation, a single colony was suspended in tryptic soy broth and agitated at 120 rpm at 37 °C until it reached the turbidity of a 0.5 McFarland Standard. The turbidity was measured using a SpectraMax spectrophotometer (Molecular Devices, San Jose, CA) and was correlated with CFU counts. Simultaneously, a standard colony count was performed on the turbid bacterial suspension.

4.18. Animal infection and treatment groups

The right cornea of each anesthetized mouse was scarified with three parallel 1 mm incisions using a sterile 25-gauge needle (5/8-in. length) under a stereomicroscope. In the prophylactic efficacy study, following the scarification, the corneas were topically treated with 1.0×10^6 CFU/cornea in a 5 μ L dose, as previously described with slight modifications [102]. The mice were then randomly assigned to one of three groups on day 0: 1) no treatment, n=8; 2) Vigamox® (MFX) eye drops (4×/day), n=8; and 3) MFX-loaded GelMAP nanosuspension (1×/day), n=9. After 3-day treatment, corneas were harvested for bacterial enumeration.

In the treatment efficacy study, following the scarification, the corneas were topically treated with 1000 CFU/cornea in a 5 μL dose, as previously described with slight modifications [90]. Eyes were examined with a slit lamp prior to infection (day -1) and one-day post-infection (day 0) to ensure consistent infection across all mice before treatment. The mice were then randomly assigned to one of three treatment groups: 1) no treatment (n = 8), 2) MFX-loaded GelMAP nanosuspension, applied once on day 0 for 5 days (n = 10), or 3) Vigamox® eye drops, applied once on day 0(n = 9) for 5 days. After the treatment period, all mice were euthanized, and their corneas were harvested for analysis on day 5, unless a humane endpoint, such as corneal perforation, was reached earlier. Corneal perforation, characterized by structural damage resulting in a hole or penetration through the cornea, was observed in some untreated mice prior to the completion of the five-day period.

4.19. Slit-lamp examination

The animals were examined using a slit lamp equipped with a Topcon DC-4 digital camera attachment, and they were photographed daily to visually monitor the progression of the disease. For clinical score assessment, slit lamp images of the mice were color-coded and graded in a masked manner by an independent observer to evaluate the severity of the disease following *P. aeruginosa* infection. The clinical scores were represented using the following scale: 0 – clear or slight opacity, partially covering the pupil; 1 – slight opacity, fully covering the anterior segment; 2 – dense opacity partially or fully covering the pupil; 3 – dense opacity covering the anterior segment; and 4 – corneal perforation. ImageJ software was utilized to quantify the opacity area and the total corneal area. The percentage of opacity area (% per cornea) was calculated by dividing the opacity area by the total corneal area.

4.20. Quantitation of viable bacteria in cornea

Individual corneas from five mice per group were homogenized in 500 μ L of sterile DPBS. Following homogenization, the supernatants were collected by centrifugation at 1000 rpm for 1 min. Aliquots of the supernatants were then cultured after serial dilutions on 5 % sheep blood agar plates in duplicate at 37 °C. The plates were incubated for 18 h at the same temperature. After incubation, the CFUs from the homogenized corneas were quantified, and the results were expressed as log10 (CFU + 1) per cornea.

4.21. Histopathology analysis

For histopathological examination, eyes from three mice per group (n=3/group) were enucleated 5 days post-treatment. The entire eyes were harvested from the mice, fixed in 4 % paraformaldehyde, embedded in paraffin, and sectioned. Histology slides were stained with H&E to visualize ocular structures.

4.22. Statistical analysis

Quantitative data were presented as mean \pm standard deviation (SD), and significance levels are denoted as follows: * (or #) p < 0.05, **p < 0.01, ***p < 0.001, and ****p < 0.0001. The corneal CFUs from each mouse in the efficacy studies were converted to log values (i.e. 10^5 CFU was converted to 5) using a log10 (CFU + 1) transformation, a standard practice in microbiological studies [103]. Comparisons between multiple groups were conducted using the GraphPad Prism 10.1.2 software with a t-test, one-way or two-way ANOVA analysis. Kruskal-Wallis ANOVA for non-continuous data (namely clinical sores). Each experiment included a minimum of three samples.

CRediT authorship contribution statement

Yuting Zheng: Writing – review & editing, Writing – original draft, Visualization, Validation, Supervision, Project administration, Methodology, Investigation, Formal analysis, Data curation, Conceptualization. Liangju Kuang: Writing – review & editing, Writing – original draft, Validation, Methodology, Investigation, Formal analysis, Data curation. Cathy Lu: Investigation, Data curation. Steven Vo: Writing – review & editing, Validation, Data curation. Akitomo Narimatsu: Investigation, Data curation. Zhonghong Kong: Data curation. Reza Dana: Writing – review & editing, Validation, Supervision, Project administration, Methodology, Investigation, Funding acquisition, Conceptualization. Nasim Annabi: Writing – review & editing, Validation, Supervision, Resources, Project administration, Methodology, Investigation, Funding acquisition, Conceptualization.

Declaration of competing interest

The authors declare the following financial interests/personal relationships which may be considered as potential competing interests: Prof Annabi and Prof Dana hold equity in GelMEDIX Inc.

Acknowledgement

We acknowledge Vy Tran and Cristopher Navarro for the illustrations of this work. We thank Dr. Francesca Kahale for her assistance with the slit lamp photography, Ms. Ann Yung for her assistance with mouse tissue pretreatment and bacterial culture, and Dr. Paulo Jose Bispo and Ms. Nicole L. Belanger for their advice on bacterial culture and *in vivo* experiments. We acknowledge Dr. Yavuz Oz for taking TEM images of the GelMAP NPs. We acknowledge Yimin Gu for helping with operating the fluorescent spectrometer. This work was supported by the Department of Defense (DOD), Vision Research Program (VRP), Investigator-Initiated Research Award (W81XWH-21-1-0869), and National Eye Institute/National Institutes of Health Core Grant for Vision Research (P30EY003790).

Appendix A. Supplementary data

Supplementary data to this article can be found online at https://doi.org/10.1016/j.jconrel.2025.114046.

Data availability

Data will be made available on request.

References

- [1] Z. Ayehubizu, W. Mulu, F. Biadglegne, Common bacterial causes of external ocular infections, associated risk factors and antibiotic resistance among patients at ophthalmology unit of Felege Hiwot Referral Hospital, Northwest Ethiopia: a cross-sectional study, J. Ophthalmic Inflam. Infect. 11 (2021) 1–10.
- [2] D. Ting, C. Ho, R. Deshmukh, D. Said, H. Dua, Infectious keratitis: an update on epidemiology, causative microorganisms, risk factors, and antimicrobial resistance, Eye (Lond.) 35 (2021) 1084–1101.
- [3] N. Congdon, D. Friedman, T. Lietman, Important causes of visual impairment in the world today, JAMA 290 (2003) 2057–2060.
- [4] M. Teweldemedhin, H. Gebreyesus, A. Atsbaha, S. Asgedom, M. Saravanan, Bacterial profile of ocular infections: a systematic review, BMC Ophthalmol. 17 (2017) 212.
- [5] C. Lakkis, K. Lorenz, M. Mayers, Topical review: contact lens eye health and safety considerations in government policy development, Optom. Vis. Sci. 99 (2022) 737–742.
- [6] P. Karpecki, M.R. Paterno, T.L. Comstock, Limitations of current antibiotics for the treatment of bacterial conjunctivitis, Optom. Vis. Sci. 87 (2010) 908–919.
- [7] S. Ghafoorianfar, A. Ghorani-Azam, S. Mohajeri, D. Farzin, Efficiency of nanoparticles for treatment of ocular infections: systematic literature review, J. Drug Deliv. Sci. Technol. 57 (2020) 101765.
- [8] A. Patel, K. Cholkar, V. Agrahari, A. Mitra, Ocular drug delivery systems: an overview, World J. Pharmacol. 2 (2013) 47–64.

- [9] H. Mochizuki, M. Yamada, S. Hatou, K. Tsubota, Turnover rate of tear-film lipid layer determined by fluorophotometry, Br. J. Ophthalmol. 93 (2009) 1535–1538.
- [10] M. Dhaval, J. Devani, R. Parmar, M. Soniwala, J. Chavda, Formulation and optimization of microemulsion based sparfloxacin in-situ gel for ocular delivery: in vitro and ex vivo characterization, J. Drug Deliv. Sci. Technol. 55 (2020) 101373.
- [11] P. Furrer, J. Mayer, R. Gurny, Ocular tolerance of preservatives and alternatives, Eur. J. Pharm. Biopharm. 53 (2002) 263–280.
- [12] C. Alvarez-Lorenzo, S. Anguiano-Igea, A. Varela-García, M. Vivero-Lopez, A. Concheiro, Bioinspired hydrogels for drug-eluting contact lenses, Acta Biomater. 84 (2019) 49–62.
- [13] L.-J. Luo, D.D. Nguyen, C.-C. Huang, J.-Y. Lai, Therapeutic hydrogel sheets programmed with multistage drug delivery for effective treatment of corneal abrasion, Chem. Eng. J. 429 (2022) 132409.
- [14] G. Chouhan, R. Moakes, M. Esmaeili, L. Hill, F. deCogan, J. Hardwicke, S. Rauz, A. Logan, L. Grover, A self-healing hydrogel eye drop for the sustained delivery of decorin to prevent corneal scarring, Biomaterials 210 (2019) 41–50.
- [15] J.-Y. Lai, L.-J. Luo, D.D. Nguyen, Multifunctional glutathione-dependent hydrogel eye drops with enhanced drug bioavailability for glaucoma therapy, Chem. Eng. J. 402 (2020) 126190.
- [16] A. Josyula, R. Omiadze, K. Parikh, P. Kanvinde, M. Appell, P. Patel, H. Saeed, Y. Sutar, N. Anders, P. He, P. McDonnell, J. Hanes, A. Date, L. Ensign, An ionpaired moxifloxacin nanosuspension eye drop provides improved prevention and treatment of ocular infection, Bioeng, Transl. Med. 6 (2021) e10238.
- [17] C.J. Yang, D.D. Nguyen, J.Y. Lai, Poly(l-histidine)-mediated on-demand therapeutic delivery of roughened ceria nanocages for treatment of chemical eye injury, Adv. Sci. (Weinh) 10 (2023) e2302174.
- [18] S. Ghosh, Y.H. Su, C.J. Yang, J.Y. Lai, Design of highly adhesive urchin-like gold nanostructures for effective topical drug administration and symptomatic relief of corneal dryness (vol 6, e240048, 2025), Small Struct. 6 (2025) 2400484.
- [19] D.D. Nguyen, J.-Y. Lai, Advancing the stimuli response of polymer-based drug delivery systems for ocular disease treatment, Polym. Chem. 11 (2020) 6988–7008.
- [20] A. Mateo Orobia, J. Saa, A. Ollero Lorenzo, J. Herreras, Combination of hyaluronic acid, carmellose, and osmoprotectants for the treatment of dry eye disease, Clin. Ophthalmol. (2018) 453–461.
- [21] C. Lynch, P. Kondiah, Y. Choonara, L. Du Toit, N. Ally, V. Pillay, Hydrogel biomaterials for application in ocular drug delivery, Front. Bioeng. Biotechnol. 8 (2020) 228.
- [22] J. Yang, H. Yu, L. Wang, J. Liu, X. Liu, Y. Hong, Y. Huang, S. Ren, Advances in adhesive hydrogels for tissue engineering, Eur. Polym. J. 172 (2022) 111241.
- [23] I.A. Khalil, B. Saleh, D. Ibrahim, C. Jumelle, A. Yung, R. Dana, N. Annabi, Ciprofloxacin-loaded bioadhesive hydrogels for ocular applications, Biomater Sci-Uk 8 (2020) 5196–5209.
- [24] C. Bertens, M. Gijs, F. van den Biggelaar, R. Nuijts, Topical drug delivery devices: a review, Exp. Eye Res. 168 (2018) 149–160.
- [25] C.-J. Yang, A. Anand, C.-C. Huang, J.-Y. Lai, Unveiling the power of gabapentin-loaded nanoceria with multiple therapeutic capabilities for the treatment of dry eye disease, ACS Nano 17 (2023) 25118–25135.
- [26] M. Kalam, M. Iqbal, A. Alshememry, M. Alkholief, A. Alshamsan, Development and evaluation of chitosan nanoparticles for ocular delivery of Tedizolid phosphate, Molecules 27 (2022) 2326.
- [27] N. Silva, S. Silva, B. Sarmento, M. Pintado, Chitosan nanoparticles for daptomycin delivery in ocular treatment of bacterial endophthalmitis, Drug Deliv. 22 (2015) 885–893
- [28] S. Ameeduzzafar, S. Abbas Imam, J. Bukhari, A. Ali Ahmad, Formulation and optimization of levofloxacin loaded chitosan nanoparticle for ocular delivery: invitro characterization, ocular tolerance and antibacterial activity, Int. J. Biol. Macromol. 108 (2018) 650–659.
- [29] S. Taghe, S. Mirzaeei, Preparation and characterization of novel, mucoadhesive ofloxacin nanoparticles for ocular drug delivery, Braz. J. Pharm. Sci. 55 (2019).
- [30] E. Krisanti, S. Aryani, K. Mulia, Effect of chitosan molecular weight and composition on mucoadhesive properties of mangostin-loaded chitosan-alginate microparticles, in: AIP Conference Proceedings, AIP Publishing, 2017.
- [31] X. Sun, Y. Sheng, K. Li, S. Sai, J. Feng, Y. Li, J. Zhang, J. Han, B. Tian, Mucoadhesive phenylboronic acid conjugated chitosan oligosaccharide-vitamin E copolymer for topical ocular delivery of voriconazole: synthesis, in vitro/vivo evaluation, and mechanism, Acta Biomater. 138 (2022) 193–207.
- [32] A. Zamboulis, S. Nanaki, G. Michailidou, I. Koumentakou, M. Lazaridou, N. Ainali, E. Xanthopoulou, D. Bikiaris, Chitosan and its derivatives for ocular delivery formulations: recent advances and developments, Polymers 12 (2020) 1519.
- [33] M. Nikzamir, A. Akbarzadeh, Y. Panahi, An overview on nanoparticles used in biomedicine and their cytotoxicity, J. Drug Deliv. Sci. Technol. 61 (2021) 102316
- [34] X. Gong, Y. Gao, J. Shu, C. Zhang, K. Zhao, Chitosan-based nanomaterial as immune adjuvant and delivery carrier for vaccines, Vaccines 10 (2022) 1906.
- [35] D. Hühn, K. Kantner, C. Geidel, S. Brandholt, I. De Cock, S. Soenen, P. Rivera-Gil, J. Montenegro, K. Braeckmans, K. Müllen, G. Nienhaus, M. Klapper, W. Parak, Polymer-coated nanoparticles interacting with proteins and cells: focusing on the sign of the net charge, ACS Nano 7 (2013) 3253–3263.
- [36] S. Liu, C. Chang, M. Verma, D. Hileeto, A. Muntz, U. Stahl, J. Woods, L. Jones, F. Gu, Phenylboronic acid modified mucoadhesive nanoparticle drug carriers facilitate weekly treatment of experimentally induced dry eye syndrome, Nano Res 8 (2015) 621–635.

- [37] G. Prosperi-Porta, S. Kedzior, B. Muirhead, H. Sheardown, Phenylboronic-acid-based polymeric micelles for mucoadhesive anterior segment ocular drug delivery, Biomacromolecules 17 (2016) 1449–1457.
- [38] G. Tan, J. Li, Y. Song, Y. Yu, D. Liu, W. Pan, Phenylboronic acid-tethered chondroitin sulfate-based mucoadhesive nanostructured lipid carriers for the treatment of dry eye syndrome, Acta Biomater. 99 (2019) 350–362.
- [39] M. Surendranath, M. Rekha, R. Parameswaran, Recent advances in functionally modified polymers for mucoadhesive drug delivery, J. Mater. Chem. B 10 (2022) 5913–5924.
- [40] S. Liu, L. Jones, F. Gu, Development of mucoadhesive drug delivery system using phenylboronic acid functionalized poly (D, L-lactide)-b-dextran nanoparticles, Macromol. Biosci. 12 (2012) 1622–1626.
- [41] Y. Zheng, A. Baidya, N. Annabi, Molecular design of an ultra-strong tissue adhesive hydrogel with tunable multifunctionality, Bioact. Mater. 29 (2023) 214–229
- [42] W. Xie, Y. Zhang, J. Zhang, X. Chen, J. Pan, X. Zhu, G. Pan, Dynamically crosslinked protien hydrogel composite as multifunctional wound dressing for cutaneous infection, Colloid Interface Sci Commun 50 (2022) 100654.
- [43] O.V. Mikhailov, Gelatin as it is: history and modernity, Int. J. Mol. Sci. 24 (2023).
- [44] S. Xu, X. Tang, M. Wang, Z. Wang, R. Zhan, J. Chen, Stimuli-responsive hydrogels composed of modified cellulose nanocrystal and gelatin with oriented channels for guiding axonal myelination, Carbohydr. Polym. 356 (2025) 123402.
- [45] S. Liu, L. Jones, F.X. Gu, Development of mucoadhesive drug delivery system using phenylboronic acid functionalized poly(D,L-lactide)-b-dextran nanoparticles, Macromol. Biosci. 12 (2012) 1622–1626.
- [46] S.K. Filippov, R. Khusnutdinov, A. Murmiliuk, W. Inam, L.Y. Zakharova, H. Zhang, V.V. Khutoryanskiy, Dynamic light scattering and transmission electron microscopy in drug delivery: a roadmap for correct characterization of nanoparticles and interpretation of results, Mater. Horiz. 10 (2023) 5354–5370.
- [47] Z. Liu, J. Mao, W. Li, C. Xu, A. Lao, A. Shin, J. Wu, A. Gu, Z. Zhang, L. Mao, K. Lin, J. Liu, Smart glucose-responsive hydrogel with ROS scavenging and homeostasis regulating properties for diabetic bone regeneration, Chem. Eng. J. 497 (2024) 154433
- [48] H.-D. Chou, C.-A. Chen, H.-Y. Liu, S.-J. Liu, P.-L. Lai, W.-C. Wu, Y.-S. Hwang, K.-J. Chen, T.-T. Tsai, C.-C. Lai, Synthesis, properties, and biocompatibility of 4-carboxyphenyboronic acid-modified gelatin-methacryloyl: a hydrogel for retinal surgeries, ACS Omega 9 (2024) 42147–42158.
- [49] V. Patel, Y. Agrawal, Nanosuspension: an approach to enhance solubility of drugs, J. Adv. Pharm. Technol. Res. 2 (2011) 81–87.
- [50] A. Albanese, P.S. Tang, W.C. Chan, The effect of nanoparticle size, shape, and surface chemistry on biological systems, Annu. Rev. Biomed. Eng. 14 (2012) 1–16.
- [51] A. Safaei-Yaraziz, S. Akbari-Birgani, N. Nikfarjam, Porous scaffolds with the structure of an interpenetrating polymer network made by gelatin methacrylated nanoparticle-stabilized high internal phase emulsion polymerization targeted for tissue engineering, RSC Adv. 11 (2021) 22544–22555.
- [52] F. Madani, S. Esnaashari, B. Mujokoro, F. Dorkoosh, M. Khosravani, M. Adabi, Investigation of effective parameters on size of paclitaxel loaded PLGA nanoparticles, Adv. Pharm. Bull. 8 (2018) 77–84.
- [53] P. Simmons, J. Vehige, Investigating the potential benefits of a new artificial tear formulation combining two polymers, Clin. Ophthalmol. (2017) 1637–1642.
- [54] U. Doshi, J. Xu, Effect of viscosity, surface tension and mucoadhesion on ocular residence time of lubricant eye drops, Invest. Ophthalmol. Vis. Sci. 50 (2009) 4641
- [55] J. Paugh, A. Nguyen, H. Ketelson, M. Christensen, D. Meadows, Precorneal residence time of artificial tears measured in dry eye subjects, Optom. Vis. Sci. 85 (2008) 725–731.
- [56] W. Prather, J. Stoecker, J. Vehige, P. Simmons, Clinical performance of a new mid-viscosity artificial tear for dry eye treatment, Invest. Ophthalmol. Vis. Sci. 43 (2002) 3152.
- [57] W. Kapadia, N. Qin, P. Zhao, C. Phan, L. Haines, L. Jones, C. Ren, Shear-thinning and temperature-dependent viscosity relationships of contemporary ocular lubricants, Transl. Vision Sci. Technol. 11 (2022) 1.
- [58] A. Maleki, A. Kjøniksen, B. Nyström, Anomalous viscosity behavior in aqueous solutions of hyaluronic acid, Polym. Bull. 59 (2007) 217–226.
- [59] E. Mašková, K. Kubová, B. Raimi-Abraham, D. Vllasaliu, E. Vohlídalová, J. Turánek, J. Mašek, Hypromellose–a traditional pharmaceutical excipient with modern applications in oral and oromucosal drug delivery, J. Control. Release 324 (2020) 695–727.
- [60] M. Labetoulle, F. Chiambaretta, A. Shirlaw, R. Leaback, C. Baudouin, Osmoprotectants, carboxymethylcellulose and hyaluronic acid multi-ingredient eye drop: a randomised controlled trial in moderate to severe dry eye, Eye (Lond.) 31 (2017) 1409–1416.
- [61] J. Tauber, Efficacy, tolerability and comfort of a 0.3% hypromellose gel ophthalmic lubricant in the treatment of patients with moderate to severe dry eye syndrome, Curr. Med. Res. Opin. 23 (2007) 2629–2636.
- [62] O. Mysen, L. Hynnekleiv, M. Magnø, J. Vehof, T. Utheim, Review of hydroxypropyl methylcellulose in artificial tears for the treatment of dry eye disease, Acta Opthalmol. 102 (2024) 881–896.
- [63] P. Aragona, P. Simmons, H. Wang, T. Wang, Physicochemical properties of hyaluronic acid-based lubricant eye drops, Transl. Vision Sci. Technol. 8 (2019) 2.
- [64] W. Gensheimer, D. Kleinman, M. Gonzalez, D. Sobti, E. Cooper, G. Smits, A. Loxley, M. Mitchnick, J. Aquavella, Novel formulation of glycerin 1% artificial tears extends tear film break-up time compared with Systane lubricant eye drops, J. Ocul. Pharmacol. Ther. 28 (2012) 473–478.

- [65] A. Youssef, R. Thakkar, S. Senapati, P. Joshi, N. Dudhipala, S. Majumdar, Design of topical moxifloxacin mucoadhesive nanoemulsion for the management of ocular bacterial infections, Pharmaceutics 14 (2022) 1246.
- [66] F. Zhang, S. Xu, Z. Wang, Pre-treatment optimization and properties of gelatin from freshwater fish scales, Food Bioprod. Process. 89 (2011) 185–193.
- [67] B. Lee, Z. Li, D. Clemens, B. Dillon, A. Hwang, J. Zink, M. Horwitz, Redox-triggered release of moxifloxacin from mesoporous silica nanoparticles functionalized with disulfide snap-tops enhances efficacy against pneumonic tularemia in mice, Small 12 (2016) 3690–3702.
- [68] S. Maldonado, M. Irún, L. Campos, J. Rubio, A. Luquita, A. Lostao, R. Wang, B. García-Moreno E, J. Sancho, Salt-induced stabilization of apoflavodoxin at neutral pH is mediated through cation-specific effects, Protein Sci. 11 (2002) 1260–1273.
- [69] L. da Rocha, A. Baptista, S. Campos, Approach to study pH-dependent protein association using constant-pH molecular dynamics: application to the dimerization of β-lactoglobulin, J. Chem. Theory Comput. 18 (2022) 1982–2001.
- [70] X. Chen, S. Gholizadeh, M. Ghovvati, Z. Wang, M. Jellen, A. Mostafavi, R. Dana, N. Annabi, Engineering a drug eluting ocular patch for delivery and sustained release of anti-inflammatory therapeutics, AICHE J. 69 (2023) e18067.
- [71] J. Huang, J. Zhong, G. Chen, Z. Lin, Y. Deng, Y.L. Liu, P.Y. Cao, B. Wang, Y. Wei, T. Wu, J. Yuan, G. Jiang, A hydrogel-based hybrid theranostic contact lens for fungal keratitis, ACS Nano 10 (2016) 6464–6473.
- [72] Y. Gao, J. Zuo, N. Bou-Chacra, J. Pinto Tde, S.D. Clas, R.B. Walker, R. Lobenberg, In vitro release kinetics of antituberculosis drugs from nanoparticles assessed using a modified dissolution apparatus, Biomed. Res. Int. 2013 (2013) 136590.
- [73] H.L. Bui, Y.-H. Su, C.-J. Yang, C.-J. Huang, J.-Y. Lai, Mucoadhesive, antioxidant, and lubricant catechol-functionalized poly(phosphobetaine) as biomaterial nanotherapeutics for treating ocular dryness, J. Nanobiotechnol. 22 (2024) 160.
- [74] P.-H. Lin, H.-J. Jian, Y.-J. Li, Y.-F. Huang, A. Anand, C.-C. Huang, H.-J. Lin, J.-Y. Lai, Alleviation of dry eye syndrome with one dose of antioxidant, anti-inflammatory, and mucoadhesive lysine-carbonized nanogels, Acta Biomater. 141 (2022) 140–150.
- [75] A. Ludwig, The use of mucoadhesive polymers in ocular drug delivery, Adv. Drug Deliv. Rev. 57 (2005) 1595–1639.
- [76] R. Dave, T. Goostrey, M. Ziolkowska, S. Czerny-Holownia, T. Hoare, H. Sheardown, Ocular drug delivery to the anterior segment using nanocarriers: a mucoadhesive/mucopenetrative perspective, J. Control. Release 336 (2021) 71 09
- [77] N. Mangiacotte, G. Prosperi-Porta, L. Liu, M. Dodd, H. Sheardown, Mucoadhesive nanoparticles for drug delivery to the anterior eye, Nanomaterials 10 (2020) 1400
- [78] M. Shin, K. Kim, W. Shim, J.W. Yang, H. Lee, Tannic acid as a degradable mucoadhesive compound, ACS Biomater. Sci. Eng. 2 (2016) 687–696.
- [79] Y.B. Choy, J.-H. Park, B.E. McCarey, H.F. Edelhauser, M.R. Prausnitz, Mucoadhesive microdiscs engineered for ophthalmic drug delivery: effect of particle geometry and formulation on preocular residence time, Invest. Ophthalmol. Vis. Sci. 49 (2008) 4808–4815.
- [80] I.S. Bayer, Recent advances in mucoadhesive Interface materials, mucoadhesion characterization, and technologies, Adv. Mater. Interfaces 9 (2022) 2200211.
- [81] D. Patel, J. Smith, A. Smith, N. Grist, P. Barnett, J. Smart, An atomic force microscopy investigation of bioadhesive polymer adsorption onto human buccal cells, Int. J. Pharm. 200 (2000) 271–277.
- [82] M. Shin, K. Kim, W. Shim, J. Yang, H. Lee, Tannic acid as a degradable mucoadhesive compound, ACS Biomater. Sci. Eng. 2 (2016) 687–696.
- [83] S.C. Baos, D.B. Phillips, L. Wildling, T.J. McMaster, M. Berry, Distribution of sialic acids on mucins and gels: a defense mechanism, Biophys. J. 102 (2012) 176–184.
- [84] Y. Nakamura, N. Yokoi, H. Tokushige, S. Kinoshita, Sialic acid in normal human tear fluid, Jpn. J. Ophthalmol. 45 (2001) 327–331.
- [85] F. Bongiovi, G. Di Prima, F. Palumbo, M. Licciardi, G. Pitarresi, G. Giammona, Hyaluronic acid-based micelles as ocular platform to modulate the loading, release, and corneal permeation of corticosteroids, Macromol. Biosci. 17 (2017) 1700261.
- [86] I.A. Khalil, B. Saleh, D.M. Ibrahim, C. Jumelle, A. Yung, R. Dana, N. Annabi, Ciprofloxacin-loaded bioadhesive hydrogels for ocular applications, Biomater Sci-Uk 8 (2020) 5196–5209.
- [87] D.C. Hooper, G.A. Jacoby, Topoisomerase inhibitors: fluoroquinolone mechanisms of action and resistance, Cold Spring Harb. Perspect. Med. 6 (2016) a025320.
- [88] N. Lall, C. Henley-Smith, M. De Canha, C. Oosthuizen, D. Berrington, Viability reagent, prestoblue, in comparison with other available reagents, utilized in cytotoxicity and antimicrobial assays, Int. J. Microbiol. 2013 (2013) 420601.
- [89] B. Wispelwey, Clinical implications of pharmacokinetics and pharmacodynamics of fluoroquinolones, Clin. Infect. Dis. 41 (Suppl. 2) (2005) S127–S135.
- [90] A. Thakur, R. Barrett, J. Hobden, L. Hazlett, Caspase-1 inhibitor reduces severity of Pseudomonas aeruginosa keratitis in mice, Investig. Ophthalmol. Vis. Sci. 45 (2004) 3177–3184.
- [91] M. Kwong, D. Evans, M. Ni, B. Cowell, S. Fleiszig, Human tear fluid protects against Pseudomonas aeruginosa keratitis in a murine experimental model, ASM J. 75 (2007) 2325–2332.
- [92] A. Salama, M. AbouSamra, G. Awad, S. Mansy, Promising bioadhesive ofloxacin-loaded polymeric nanoparticles for the treatment of ocular inflammation: formulation and in vivo evaluation, Drug Deliv. Transl. Res. 11 (2021) 1042 1057.
- [93] S. Padaga, H. Bhatt, S. Ch, M. Paul, A. Itoo, B. Ghosh, S. Roy, S. Biswas, Glycol chitosan-poly(lactic acid) conjugate nanoparticles encapsulating ciprofloxacin: a

- mucoadhesive, antiquorum-sensing, and biofilm-disrupting treatment modality for bacterial keratitis, ACS Appl. Mater. Interfaces 16 (2024) 18360–18385.
- [94] M. Malani, A. Thodikayil, S. Saha, J. Nirmal, Carboxylated nanofibrillated cellulose empowers moxifloxacin to overcome Staphylococcus aureus biofilm in bacterial keratitis, Carbohydr. Polym. 324 (2024) 121558.
- [95] H. Hassan, A. Ali, E. ElDesawy, A. ElShafeey, Pharmacokinetic and pharmacodynamic evaluation of gemifloxacin chitosan nanoparticles as an antibacterial ocular dosage form, J. Pharm. Sci. 111 (2022) 1497–1508.
- [96] X. Kong, Y. Jia, H. Wang, R. Li, C. Li, S. Cheng, T. Chen, Y. Mai, Y. Nie, Y. Deng, Z. Xie, Y. Liu, Effective treatment of Haemophilus influenzae-induced bacterial conjunctivitis by a bioadhesive nanoparticle reticulate structure, ACS Appl. Mater. Interfaces 15 (2023) 22892–22902.
- [97] Q. Chen, X. Han, L. Liu, Y. Duan, Y. Chen, L. Shi, Q. Lin, L. Shen, Multifunctional polymer vesicles for synergistic antibiotic–antioxidant treatment of bacterial keratitis, Biomacromolecules 24 (2023) 5230–5244.
- [98] K. Yue, G. Trujillo-de Santiago, M. Alvarez, A. Tamayol, N. Annabi, A. Khademhosseini, Synthesis, properties, and biomedical applications of gelatin methacryloyl (GelMA) hydrogels, Biomaterials 73 (2015) 254–271.

- [99] K. Kimura, K. Yamasaki, H. Nakamura, M. Haratake, K. Taguchi, M. Otagiri, Preparation and in vitro analysis of human serum albumin nanoparticles loaded with anthracycline derivatives, Chem. Pharm. Bull. 66 (2018) 382–390.
- [100] B. Srividya, R. Cardoza, P.D. Amin, Sustained ophthalmic delivery of ofloxacin from a pH triggered in situ gelling system, J. Control. Release 73 (2001) 205–211.
- [101] J. Byers, J. Sarver, Chapter 10 pharmacokinetic modeling, in: M. Hacker, W. Messer, K. Bachmann (Eds.), Pharmacology, Academic Press, San Diego, 2009, pp. 201–277.
- [102] A. Thakur, R.P. Barrett, J.A. Hobden, L.D. Hazlett, Caspase-1 inhibitor reduces severity of pseudomonas aeruginosa keratitis in mice, Invest. Ophthalmol. Vis. Sci. 45 (2004) 3177–3184.
- [103] E. Romanowski, J. Romanowski, R. Shanks, K. Yates, A. Mammen, D. Dhaliwal, V. Jhanji, R. Kowalski, Topical vancomycin 5% is more efficacious than 2.5% and 1.25% for reducing viable methicillin-resistant Staphylococcus aureus in infectious keratitis, Cornea 39 (2020) 250–253.